Letters in Mathematical Physics (2019) 109:449–495
https://doi.org/10.1007/s11005-018-1118-4

Punctures and dynamical systems

Falk Hassler[1,2] · **Jonathan J. Heckman**[2]

Received: 26 March 2018 / Revised: 20 June 2018 / Accepted: 16 July 2018 / Published online: 3 August 2018

Abstract
With the aim of better understanding the class of 4D theories generated by compactifications of 6D superconformal field theories (SCFTs), we study the structure of $\mathcal{N} = 1$ supersymmetric punctures for class $\mathcal{S}_\Gamma$ theories, namely the 6D SCFTs obtained from M5-branes probing an ADE singularity. For M5-branes probing a $\mathbb{C}^2/\mathbb{Z}_k$ singularity, the punctures are governed by a dynamical system in which evolution in time corresponds to motion to a neighboring node in an affine A-type quiver. Classification of punctures reduces to determining consistent initial conditions which produce periodic orbits. The study of this system is particularly tractable in the case of a single M5-brane. Even in this "simple" case, the solutions exhibit a remarkable level of complexity: Only specific rational values for the initial momenta lead to periodic orbits and small perturbations in these values lead to vastly different late-time behavior. Another difference from half BPS punctures of class $\mathcal{S}$ theories includes the appearance of a continuous complex "zero mode" modulus in some puncture solutions. The construction of punctures with higher-order poles involves a related set of recursion relations. The resulting structures also generalize to systems with multiple M5-branes as well as probes of D- and E-type orbifold singularities.

Keywords 6D SCFTs · Punctures · Dynamical systems · 4D SCFTs

Mathematics Subject Classification 37N20 · 17B08

Contents

1 Introduction 450
2 Punctures and dynamical systems 454

✉ Falk Hassler
fhassler@unc.edu

Jonathan J. Heckman
jheckman@sas.upenn.edu

1 Department of Physics and Astronomy, University of Pennsylvania, Philadelphia, PA 19104, USA

2 Department of Physics, University of North Carolina, Chapel Hill, NC 27599, USA

2.1 Specialization to $N = 1$ . . . 456
2.2 Periodic orbits . . . 457
3 Eternal punctures . . . 458
3.1 Rational momenta . . . 459
3.2 Zero mode . . . 460
3.3 Minimal momenta and maximal positions . . . 461
3.4 Periodic orbit conditions . . . 465
4 Terminal punctures . . . 468
4.1 Irreducible representations . . . 472
5 Higher-order poles . . . 474
6 Comments on the higher-rank case . . . 478
7 Conclusions . . . 480
A Periodic orbit proofs . . . 482
References . . . 493

1 Introduction

Compactifications of higher-dimensional theories produce a wealth of insights into the construction and study of lower-dimensional quantum field theories. In some sense, the natural starting point for addressing many issues of compactification is to start with the highest dimension quantum field theories for which supersymmetry and conformal symmetry can be combined, namely compactifications of six-dimensional superconformal field theories (6D SCFTs). The first evidence for the existence of 6D SCFTs appeared in references [1–4] (see also [5–14]), and there has recently been renewed interest in the subject, in terms of both classifying the resulting theories [15–21] and extracting non-trivial data from these theories and their compactifications [22–55].

For 4D theories obtained from 6D SCFTs, the defining data for a compactification include specifying a Riemann surface with punctures, namely marked points with prescribed boundary conditions for various operators of the 6D SCFT. A particularly clean class of examples are 4D $\mathcal{N} = 2$ theories obtained from compactifications of $\mathcal{N} = (2, 0)$ theories on Riemann surfaces with first-order poles for operators at marked points. For a class $\mathcal{S}$ theory associated with a Lie algebra $\mathfrak{g}_{ADE}$ of ADE type, the punctures are then specified by embeddings of the Lie algebra $\mathfrak{su}(2)$ in $\mathfrak{g}_{ADE}$. These are in turn characterized by nilpotent orbits in the Lie algebra $\mathfrak{g}_{ADE}$, and for A-type theories, this has a simple pictorial representation in terms of Young diagrams, as used, for example, in reference [56].

The vast number of additional 6D SCFTs with $\mathcal{N} = (1, 0)$ supersymmetry suggests a corresponding proliferation of possible 4D $\mathcal{N} = 1$ theories obtained from subsequent compactification. While it is still an open question to determine the structure of punctures in all 6D SCFTs, in the special case of the class $\mathcal{S}_\Gamma$ theories, namely M5-branes probing an ADE singularity $\mathbb{C}^2/\Gamma_{ADE}$, the defining equations for punctures have at least been worked out [25,40]. What remains to be done, however, is to develop a classification scheme for possible boundary conditions, analogous to what exists for 1/2 BPS simple punctures of class $\mathcal{S}$ theories.

To a certain extent, all of the 1/2 BPS punctures of class $\mathcal{S}_\Gamma$ theories descend from the special case of $\mathcal{N} = 1$ supersymmetric punctures of A-type class $\mathcal{S}$ theories, subject to the additional conditions imposed by a Douglas–Moore-type orbifold pro-

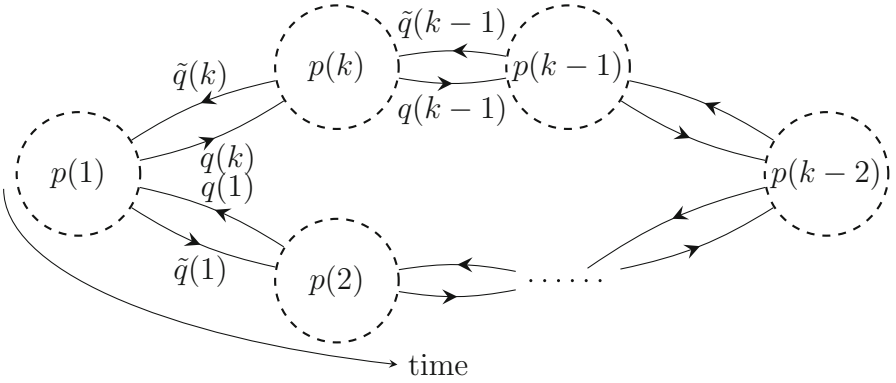

Fig. 1 A-type quiver with the direction along the quiver interpreted as the time of the dynamical system

jection [57]. In the special case of simple punctures, the 1/4 BPS puncture equations of class $\mathcal{S}$ theories are [58] (see also [25,40]):

$$[\Sigma, Q] = Q, \quad [\Sigma, \widetilde{Q}] = \widetilde{Q}, \quad [Q, \widetilde{Q}] = 0, \quad [Q, Q^\dagger] + [\widetilde{Q}, \widetilde{Q}^\dagger] = \Sigma, \tag{1.1}$$

where Σ, Q and $\widetilde{Q}$ are $N \times N$ matrices with complex entries, and Σ is Hermitian. Making the replacement $N \mapsto |\Gamma|\, N$ and also demanding these matrices transform in suitable representations of Γ then leads to $\mathcal{N} = 1$ supersymmetric punctures of class $\mathcal{S}_\Gamma$ theories [25,40]. In the special case where $[Q, \widetilde{Q}^\dagger] = 0$, the problem reduces to the study of embeddings of $\mathfrak{su}(2)^l \to \mathfrak{su}(|\Gamma|\, N)$, subject to the additional constraints of an orbifold projection. This of course prompts the question as to whether such solutions are "typical."

Our aim in this paper will be to take some preliminary steps in classifying punctures for class $\mathcal{S}_\Gamma$ theories, focusing in particular on the case of simple punctures for M5-branes probing $\mathbb{C}^2/\mathbb{Z}_k$. Some of the solutions we present also embed in the D- and E-type class $\mathcal{S}_\Gamma$ theories.

The main idea we introduce is that the puncture equations can be visualized in terms of a discrete dynamical system. Indeed, instead of working in terms of large $Nk \times Nk$ matrices, we can alternatively use a "quiver basis" in which the orbifold projection has already been imposed. In this case, depicted in Fig. 1, we can label the nodes of the quiver by an index $i = 1, \ldots, k$ and visualize this index as a time step in a discrete dynamical system. The evolution equations are, in terms of matrices $q(i)$, $\widetilde{q}(i)$ and $p(i)$, respectively, associated with the parent matrices Q, $\widetilde{Q}$ and Σ:

$$q(i) = p(i)q(i) - q(i)p(i+1), \tag{1.2}$$

$$-\widetilde{q}(i) = \widetilde{q}(i)p(i) - p(i+1)\widetilde{q}(i), \tag{1.3}$$

$$0 = q(i)\widetilde{q}(i) - \widetilde{q}(i-1)q(i-1), \tag{1.4}$$

$$p(i) = \Big[q(i)q^\dagger(i) - \widetilde{q}^\dagger(i)\widetilde{q}(i)\Big] - \Big[q^\dagger(i-1)q(i-1) - \widetilde{q}(i-1)\widetilde{q}^\dagger(i-1)\Big]. \tag{1.5}$$

So, once we know the values of the matrices at timestep i, the evolution to timestep $i+1$ is implicitly specified. A similar iteration procedure also holds for punctures with higher-order poles. In this case, there is an evolution, not just in "time" but also in "space."

Already for the case of $N = 1$ where we have a single M5-brane and an IR free theory, the structure of simple punctures generated by this dynamical system is surprisingly complex. To illustrate, we study in detail this class of solutions, obtaining a full classification of initial conditions which produce a puncture. The method also leads to a new class of punctures for interacting 6D SCFT. For example, since we can also embed these solutions inside large $N \times N$ matrices, we automatically generate $1/4$ BPS punctures for class $\mathcal{S}$ theories of A_{N-1} type. For the higher rank $N > 1$ class $\mathcal{S}_\Gamma$ theories, these solutions also embed as solutions which are diagonal block by block.

For a single M5-brane, namely $N = 1$, the form of the dynamical system is more explicit and can be fully automated. Introducing a position coordinate

$$x(i) = |q(i)|^2 - |\widetilde{q}(i)|^2 , \tag{1.6}$$

the evolution from one value of position $x(i)$ and momentum $p(i)$ to the next is:

$$\begin{bmatrix} p(i+1) \\ x(i+1) \end{bmatrix} = \begin{bmatrix} 1 & 0 \\ 1 & 1 \end{bmatrix} \begin{bmatrix} p(i) \\ x(i) \end{bmatrix} - \begin{bmatrix} \operatorname{sgn} x(i) \\ \operatorname{sgn} x(i) \end{bmatrix}, \tag{1.7}$$

where $\operatorname{sgn}(x) = x/|x|$ for $x \neq 0$ and 0 otherwise. This evolution holds provided $x(i) \neq 0$. When $x(i_*) = 0$ vanishes at some timestep, we can restart the evolution with another choice of initial condition.

Compared with other discrete dynamical systems, the appearance of the term $\operatorname{sgn}(x(i))$ leads to significant subtleties which are often only apparent in sufficiently long quivers. Among other things, the presence of this term obstructs a straightforward continuum limit, and small perturbations lead to quite different behavior at later time steps. Our goal will be to determine which initial conditions $p(1)$ and $x(1)$ actually produce viable punctures.

We show that a puncture corresponds to the special condition that the orbit eventually returns to itself, namely we have a periodic orbit. Moreover, periodic orbits are only achieved when the initial momentum $p(1)$ is a rational number, which in turn means that all other momenta are also rational and can all be expressed with same choice of denominator. So, we can write $p(i) = a(i)/b$ with $a(i)$ and b relatively prime integers. We prove that:

$$b \neq 0 \bmod 4 \Rightarrow \text{Periodic orbit.} \tag{1.8}$$

Based on extensive numerical tests, we also find that the converse holds, namely when $b = 0 \bmod 4$, that we never have a periodic orbit. In the latter case, the late-time values of the $x(i)$ become unbounded.

Returning to the system of physical punctures, we also see that one can consider "eternal punctures" where no $x(i)$ vanish and "terminal punctures" in which some of the $x(i)$ vanish. In the former case, there is really a single dynamical system which

continues for all time, while in the latter case, we can restart the dynamical system with a new initial condition after each value of i for which $x(i)$ vanishes.[1] In terms of the dynamical system, the two classes of punctures have initial conditions:

$$\text{Eternal punctures}: \quad x(1) \in \mathbb{R} \text{ and } x(1) \neq p(1) = \frac{a(1)}{b} \text{ with } b \neq 0 \bmod 4, \quad (1.9)$$

$$\text{Terminal punctures}: \quad x(1) = p(1) = \frac{a(1)}{b} \text{ with } b \neq 0 \bmod 4. \quad (1.10)$$

An interesting feature of the eternal punctures which does not appear for 1/2 BPS punctures of class $\mathcal{S}$ theories or for previously studied punctures of $\mathcal{N} = (1, 0)$ theories is the appearance of an overall zero mode: For sufficiently small δx, the initial values for the position $x(1)$ and $x(1) + \delta x$ produce the same eternal puncture. In the equations defined by a puncture, this is also accompanied by a complex phase which cannot be removed by a unitary change of basis. Note that the length of the orbit k in an eternal puncture depends on $x(1)$ and $p(1)$, so we can also write $k(x(1), p(1))$. Alternatively, we can hold fixed $p(1)$, and for the set of k's which appear, there is an interval of admissible $x(1)$'s which correspond to the same puncture.

We can reach all periodic orbits by gluing together terminal punctures and then perturbing these solutions by the small parameter δx. From this perspective, the rather special case where we embed $su(2)$ in $su(N)$ corresponds to the restricted case where b is one or two. This illustrates the vast increase in possible punctures for 4D $\mathcal{N} = 1$ vacua.

The dynamical system we encounter is also of interest in its own right, and we also analyze some additional aspects of its behavior, including sensitivity to initial conditions and number of orbits as a function of orbit length. There are fairly regular patterns for many of these quantities, indicating additional non-trivial structure.

This non-trivial structure also persists for punctures with higher-order poles, where there is again a recursion relation, this time from one pole order to the next. Once we pass beyond simple order poles, the evolution descends to a linear set of first-order discrete evolution equations rather than the second-order behavior exhibited by the first-order poles.

An important feature of the puncture solutions thus obtained is that they also generate punctures for more general 6D SCFTs. For example, in the case of N M5-branes probing an A-type singularity, the scalars q, $\widetilde{q}$ and Σ appearing in the puncture equations are promoted to $N \times N$ matrices. The particular ansatz where all such matrices are diagonal yields a large class of new punctures, each governed by a decoupled dynamical system. More ambitiously, we can also consider dynamical systems involving the full matrix structure. In this case, the appearance of a time-like evolution across quiver nodes still applies, though it is more involved. Similar considerations clearly apply for punctures of other 6D SCFTs.

The rest of this paper is organized as follows. In Sect. 2, we establish the basic connection between punctures and dynamical systems. We next turn to the classification of initial conditions for the dynamical system with $N = 1$, first studying the

[1] Note that in the dynamical system, we are of course free to simply continue past this point without restarting with a new initial condition.

case with all $x(i)$ nonzero in Sect. 3 and then turning to the case where some $x(i)$ vanish in Sect. 4. We analyze the structure of higher-order poles in Sect. 5. Section 6 discusses generalizations to the case of higher rank. We present our conclusions and potential future directions in Sect. 7. In Appendix 1, we present some formal proofs establishing which initial conditions of the dynamical system yield a periodic orbit.

2 Punctures and dynamical systems

In this section, we establish a correspondence between punctures and dynamical systems. In doing so, we reduce the problem of classification to determining which initial conditions yield a puncture.

Recall first that the $\mathcal{S}_k$ theories are given by N M5-branes probing the transverse geometry $\mathbb{R}_\perp \times \mathbb{C}^2/\mathbb{Z}_k$. Punctures for such theories are obtained by dimensionally reducing on a long cylinder $S^1 \times \mathbb{R}_{\geq 0}$. The reduction along the circle factor of the cylinder geometry produces a 5D $\mathcal{N} = 1$ gauge theory with scalar degrees of freedom given by $N \times N$ matrices of fields, Σ, Q and $\widetilde{Q}$, and we impose supersymmetry preserving boundary conditions on the semi-infinite interval. There is then a power series expansion for modes near the boundary ($t = 0$) of $\mathbb{R}_{\geq 0}$:

$$Q = \sum_{n>0} \frac{Q_n}{t_n}, \quad \widetilde{Q} = \sum_{n>0} \frac{\widetilde{Q}_n}{t^n} \quad \text{and} \quad \Sigma = \sum_{n>0} \frac{\Sigma_n}{t^n}, \tag{2.1}$$

and the puncture is governed by the matrix Eqs. [40]:

$$\begin{aligned} &\sum_{k+l=m} [\Sigma_k, Q_l] = (m-1) Q_{m-1} && \sum_{k+l=m} [Q_k, \widetilde{Q}_l] = 0 \\ &\sum_{k+l=m} [\Sigma_k, \widetilde{Q}_l] = (m-1) \widetilde{Q}_{m-1} && \sum_{k+l=m} [Q_k, Q_l^\dagger] + [\widetilde{Q}_k, \widetilde{Q}_l^\dagger] = (m-1)\Sigma_{m-1}, \end{aligned} \tag{2.2}$$

where the subscript on each matrix denotes the order of the pole.

Proceeding order by order in the poles, we see that for first-order poles, i.e., $m = 1$, we have the quadratic equations:

$$[\Sigma_1, Q_1] = Q_1, \ [\Sigma_1, \widetilde{Q}_1] = \widetilde{Q}_1, \ \ [Q_1, \widetilde{Q}_1] = 0, \ \ \Sigma_1 = [Q_1, Q_1^\dagger] + [\widetilde{Q}_1, \widetilde{Q}_1^\dagger]. \tag{2.3}$$

Since we shall mainly focus on the first-order poles, we shall drop the subscript for the Σ_1, Q_1 and $\widetilde{Q}_1$ and simply write Σ, Q and $\widetilde{Q}$, respectively.

Observe that at second order and above, the equations become linear in the corresponding pole order. In this sense, once we solve the first-order equations, all subsequent orders can be iteratively solved by linear transformations. Therefore, we can "evolve" from one pole order to the next in the generic case, and it is enough to focus on the first-order poles. Note that there are also some special cases where the series of higher poles stops at some point. We will discuss them in detail in Sect. 5.

Let us make a few comments on the space of solutions. First, we note that there is an obvious redundancy by a unitary change of basis. Two punctures lead to the same physical theory under transformations of the form:

$$\Sigma \mapsto U^\dagger \Sigma U, \quad Q \mapsto U^\dagger Q U, \quad \widetilde{Q}^\dagger \mapsto U^\dagger \widetilde{Q}^\dagger U, \tag{2.4}$$

for U a unitary matrix in $U(N)$. Note also that the pair Q and $\widetilde{Q}^\dagger$ rotate as a doublet under the $SU(2)$ R-symmetry of the parent 5D theory. This is broken to an $\mathcal{N} = 1$ subalgebra by the presence of the puncture. Counting up the total number of degrees of freedom, we have $5N^2$ real degrees of freedom, subject to $4N^2$ constraint equations, and N^2 "gauge redundancies." From this perspective, one might expect to only find a discrete point set of solutions, and in many cases, this is indeed correct. The caveat to this is that sometimes there can be residual "zero modes."

Let us now further specialize to the case of first-order poles for the class $\mathcal{S}_k$ theories. Working in terms of $Nk \times Nk$ matrices, we decompose into blocks, each of which is an $N \times N$ matrix. Applying the orbifold projection of reference [57], the surviving entries of the matrices in a "quiver basis" are given by a set of linear maps between k different N-dimensional vector spaces $V_1, \ldots, V_k$:

$$p(i) : V_i \to V_i, \quad q(i) : V_{i+1} \to V_i, \quad \widetilde{q}(i) : V_i \to V_{i+1}. \tag{2.5}$$

Embedding in the original $Nk \times Nk$ matrices, we can also write:

$$\Sigma_1 = \begin{bmatrix} p(1) & & & \\ & \ddots & & \\ & & p(k-1) & \\ & & & p(k) \end{bmatrix}, \tag{2.6}$$

$$Q_1 = \begin{bmatrix} & q(1) & & \\ & & \ddots & \\ & & & q(k-1) \\ q(k) & & & \end{bmatrix}, \tag{2.7}$$

$$\widetilde{Q}_1 = \begin{bmatrix} & & & \widetilde{q}(k) \\ \widetilde{q}(1) & & & \\ & \ddots & & \\ & & \widetilde{q}(k-1) & \end{bmatrix}. \tag{2.8}$$

The puncture equations now reduce to:

$$q(i) = p(i)q(i) - q(i)p(i+1), \tag{2.9}$$

$$-\widetilde{q}(i) = \widetilde{q}(i)p(i) - p(i+1)\widetilde{q}(i), \tag{2.10}$$

$$0 = q(i)\widetilde{q}(i) - \widetilde{q}(i-1)q(i-1), \tag{2.11}$$

$$p(i) = \left[q(i)q^\dagger(i) - \widetilde{q}^\dagger(i)\widetilde{q}(i)\right] - \left[q^\dagger(i-1)q(i-1) - \widetilde{q}(i-1)\widetilde{q}^\dagger(i-1)\right]. \tag{2.12}$$

Again, there is a redundancy in the solutions given by acting by a set of unitary matrices:

$$p(i) \mapsto U^\dagger(i)p(i)U(i), \quad q(i) \mapsto U^\dagger(i)q(i)U(i+1), \quad \widetilde{q}^\dagger \mapsto U^\dagger(i)\widetilde{q}U(i+1), \tag{2.13}$$

for $U(i)$ a unitary transformation of the vector space V_i. An important feature of this set of equations is that it is recursive in structure, namely if we possess a solution, we can iteratively solve for the matrices at node $i+1$ using the matrices at node i. In this sense, punctures always generate a dynamical system. Of course, it may prove difficult to explicitly construct solutions.

Our plan in the remainder of this section will be to study the formal structure of these puncture equations. The analytically most tractable case is $N = 1$, namely a single M5-brane probing an orbifold singularity. This already leads to a surprisingly rich structure, and one of our aims in the remainder of this paper will be to fully characterize the solutions in this special case.

2.1 Specialization to $N = 1$

To gain further understanding of the possible solutions to this system of equations, we now specialize even further to the case of $N = 1$. In this case, the matrices at each time step are just numbers, and we can write the whole system as:

$$q(i) = [p(i) - p(i+1)]\, q(i), \tag{2.14}$$

$$-\widetilde{q}(i) = [p(i) - p(i+1)]\, \widetilde{q}(i), \tag{2.15}$$

$$0 = q(i)\widetilde{q}(i) - \widetilde{q}(i-1)q(i-1), \tag{2.16}$$

$$p(i) = \left[|q(i)|^2 - |\widetilde{q}(i)|^2\right] - \left[|q(i-1)|^2 - |\widetilde{q}(i-1)|^2\right]. \tag{2.17}$$

For any time step i, at most one of $q(i)$ or $\widetilde{q}(i)$ can be nonzero (and thus line (2.16) is always satisfied). Assuming we are in the generic situation where at least one is nonzero, we fully characterize the solution by the recursion relations:

$$\begin{bmatrix} p(i+1) \\ x(i+1) \end{bmatrix} = \begin{bmatrix} 1 & 0 \\ 1 & 1 \end{bmatrix} \begin{bmatrix} p(i) \\ x(i) \end{bmatrix} - \begin{bmatrix} \operatorname{sgn} x(i) \\ \operatorname{sgn} x(i) \end{bmatrix}, \tag{2.18}$$

where

$$x(i) = |q(i)|^2 - |\widetilde{q}(i)|^2 . \tag{2.19}$$

One can also work purely in terms of a second-order relation:

$$-x(i-1) + 2x(i) - x(i+1) = \operatorname{sgn} x(i), \tag{2.20}$$

so one can visualize this as a discrete wave equation subject to a non-trivial source.

To a certain extent, even the particular values of the $x(i)$ are redundant. The only combinatorial data which actually enter in specifying the puncture are the sign of

$x(i)$. We can therefore introduce a spin variable $s(i) = \text{sgn}(x(i))$ with values ± 1 or 0 depending on whether $x(i)$ is positive, negative, or vanishes.

Now, from the perspective of finding puncture solutions, if we ever encounter a value i_* such that $x(i_*) = 0$, we can simply supply another initial condition to the dynamical system and continue evolving. Said differently, a sequence of nonzero values of $x(i)$ determines a puncture, and we can of course produce another puncture by appending to it another such sequence by restarting the dynamical system with a different choice of initial conditions.

Along these lines, we refer to a "terminal puncture" as one for which $x(k) = 0$. Additionally, there are punctures for which no value of $x(i)$ vanishes. In such situations, the fact that both parent matrices Q and $\widetilde{Q}$ are nilpotent means that there is at least one sign flip in the sequence of $x(i)$'s. We refer to this as an "eternal puncture." Summarizing, we have two types of punctures to consider:

$$\text{Terminal puncture} : x(0) = x(k) = 0, \tag{2.21}$$

$$\text{Eternal puncture} : x(i) \neq 0 \text{ for all } i = 1, \ldots, k. \tag{2.22}$$

Note that whereas for a puncture we naturally identify $x(0)$ and $x(k)$, in the context of a dynamical system, nothing forces us to do so.

Indeed, from the perspective of the dynamical system we can just study the evolution equations of line (2.18); we simply feed in a choice of initial conditions at $i = 0$, namely $p(0)$ and $x(0)$, and then proceed to evolve it for all time steps $i \in \mathbb{Z}_{\geq 0}$. In the process of this evolution, it can happen that $x(i)$ vanishes for several choices of i, and we can label this subsequence of values as $k_1, \ldots, k_m, \ldots$. Each such termination leads to a valid solution to the puncture equations for some choice of quiver size (typically different from k). In the context of the dynamical system, however, we can continue to evolve past this point of vanishing. It could even happen that the sequence hits zero at some value, but does not (yet) repeat its profile through the phase space.[2]

2.2 Periodic orbits

Even so, the only initial conditions we need concern ourselves with are those with a periodic orbit, though a priori the period length may differ from k. In the case where no $x(i)$ vanish for the puncture equations, namely we have an eternal puncture, it is clear that for us to get a solution to the puncture equations, the dynamical system must execute a periodic orbit. In the case of a terminal puncture, we recall that necessarily, such a puncture has $x(0) = 0$ and $x(k) = 0$. In terms of the $x(i)$, recall that we can express the puncture equations as a second-order discrete difference:

$$-x(i-1) + 2x(i) - x(i+1) = \text{sgn}\, x(i). \tag{2.23}$$

[2] A consequence of our analysis, however, is that if an orbit for $x(i)$ passes through zero twice then it necessarily executes a periodic orbit.

Summing from $i = k - n + 1$ to $i = k + n - 1$ for some $n \geq 1$ yields a telescoping series, so we obtain:

$$-x(k-n) - x(k+n) = \sum_{i=k-n+1}^{k+n-1} \operatorname{sgn} x(i). \tag{2.24}$$

Proceeding by induction, we see that for $n = 1$, we need to evaluate $\operatorname{sgn} x(k) = 0$, so we learn that $x(k-1) = -x(k+1)$. Assuming the relation:

$$x(k-n) + x(k+n) = 0 \tag{2.25}$$

holds for $n = 1, \ldots, N$, it clearly also holds for $n = N + 1$, since the signs on the right-hand side of line (2.24) cancel pairwise. This establishes relation (2.24) for all n. Since we essentially just run the evolution in reverse as we cross through a zero, we see that in the case of a puncture, where $x(0) = x(k) = 0$, the orbit necessarily repeats after at most $2k$ steps. That is to say, we can set $n = k - i$ to obtain:

$$x(i) = -x(2k-i) = x(2k+i), \tag{2.26}$$

where in the second equality, we used the fact that $x(2k) = 0$, so $x(2k - i) = -x(2k + i)$.

This establishes that for the analysis of punctures, it is enough to focus on periodic orbits of the dynamical system. Additionally, we see that even if $x(0) = x(k) = 0$, the length of the orbit may be $2k$ rather than k. We reference these two possibilities as "short orbits" and "long orbits":

$$\text{Short orbit : Period of length } k, \tag{2.27}$$

$$\text{Long orbit : Period of length } 2k. \tag{2.28}$$

Note that eternal punctures always come from short orbits, whereas a terminal puncture could be either a short or long orbit.

Now, because we have a trajectory which repeats after at most $2k$ steps, we see at once that the momenta must be quantized in units of $1/k$ or $1/2k$. The only case which corresponds to representations of $\mathfrak{su}(2)$ is the very special case where the momenta is a half integer or an integer.

We now turn to the initial conditions necessary for our dynamical system to execute a periodic orbit.

3 Eternal punctures

Our aim in this section will be to determine initial conditions which produce eternal puncture. A helpful feature of this case is that there is a natural geometric interpretation of the solutions. To see this, we return to the large matrices Q and $\widetilde{Q}$, which are interpreted as the matrix collective coordinates for branes moving on the space $\mathbb{C}^2/\Gamma$.

Now, although these matrices are nilpotent, we see that for an eternal puncture, the combinations:

$$Q_{\pm} = Q \pm \widetilde{Q}^{\dagger} \tag{3.1}$$

have non-vanishing determinant. Indeed, note that since:

$$\mathrm{Tr}(Q_{\pm}^{j}) = 0 \quad \text{for} \quad 1 \leq j < k, \tag{3.2}$$

we also learn that the eigenvalues of Q_+ and Q_- are:

$$\mathrm{Eigen}(Q_+) = \mathrm{Eigen}(Q_-) = \left\{ \zeta \times \prod_{i=1}^{k} (q(i) \pm \widetilde{q}^{\dagger}(i)) \quad \text{s.t.} \quad \zeta^k = 1 \right\}. \tag{3.3}$$

Here, we have used the fact that there must be an even number of sign flips in the $x(i)$, since the momentum needs to return to its initial value after k time steps.

Even so, we must exercise some caution with our geometric interpretation because the coordinates Q_+ and Q_- do not commute. There is a sense in which we have a semi-classical limit, however, because we can consider the special limit where the rank of $[Q_+, Q_-]$ is much smaller than k. In this case, the relative number of total sign flips is also quite small.

The rest of this section is organized as follows. First, we show that for an orbit of length k, the momenta is quantized in units of $1/k$. Additionally, we show that in this case, there is no quantization in the value of the $x(i)$'s, and in fact, that there is an overall zero mode for the system. We then turn to a detailed analysis of the dynamical system associated with eternal punctures, showing in particular that for nearly all values of the momenta, we do indeed obtain a periodic orbit. There are, however, a few cases which do not appear to exhibit this structure, corresponding to the special cases where $p(1) = a/b$ for $b = 0 \bmod 4$.

3.1 Rational momenta

The first non-trivial observation we can make is that the momenta of the system necessarily take values in the rational numbers. To see this, consider again the kth iteration of the dynamical system:

$$p(k+1) = p(1) - \sum_{i=1}^{k} \mathrm{sgn}\, x(i), \tag{3.4}$$

$$x(k+1) = kp(1) + x(1) - \sum_{i=1}^{k} (k-i)\mathrm{sgn}\, x(i). \tag{3.5}$$

On the other hand, since we have assumed $x(k+1) = x(1)$, the second line already tells us that $p(1)$ is a rational number such that $kp(1)$ is an integer:

$$p(1) = \frac{1}{k}\sum_{i=1}^{k}(k-i)\text{sgn}\, x(i). \tag{3.6}$$

The challenge, of course, is that we do not a priori know which signs for $x(i)$ will yield a consistent solution to the dynamical system. Note also that there is a priori no reason for the $x(i)$ to take values in the rational numbers.

3.2 Zero mode

Indeed, the dynamical system leaves unfixed an overall "zero mode." Suppose that we have managed to find a consistent choice of initial conditions for $x(1)$ and $p(1)$ which solves the conditions of the dynamical system. Now, for δx sufficiently small, we can perturb each of the $x(i)$ so that we do not change the sign of any $x(i)$:

$$x(i) \mapsto x(i) + \delta x \quad \text{with} \quad \text{sgn}\, x(i) = \text{sgn}(x(i) + \delta x). \tag{3.7}$$

Observe that because only the differences of $x(i)$ show up in this system, this "zero mode" in fact decouples. So in general, there is a small continuous modulus associated with eternal punctures. Additionally, we see that whereas the momentum is naturally quantized, the position can in principle take on arbitrary real values.

An additional comment is that there is also an unfixed overall phase for the $q(i)$ and $\widetilde{q}^{\dagger}(i)$. By a choice of unitary transformation, we can map each $q(i) + \widetilde{q}^{\dagger}(i)$ to:

$$\left(q(i) + \widetilde{q}^{\dagger}(i)\right) \mapsto U(i)\left(q(i) + \widetilde{q}^{\dagger}(i)\right)U^{\dagger}(i+1) \tag{3.8}$$

for some choice of complex phases $U(i)$. Doing so, we can eliminate most of the phases using the constraints:

$$\arg(U(i)U^{\dagger}(i+1)) = -\arg(q(i) + \widetilde{q}^{\dagger}(i)), \tag{3.9}$$

so there is one overall phase which cannot be eliminated by a change of basis. This is in some sense the "bosonic partner" to the radial mode δx, as one would expect in an $\mathcal{N} = 1$ supersymmetric theory. Whereas the complex phase of the q and $\widetilde{q}$'s completely decouples from our analysis, we will see that suitable tuning of δx allows us to interpolate from eternal punctures to terminal punctures. For higher values of N, we anticipate that in general, the corresponding "zero modes" can also mix, so that the matrices cease to remain diagonal.

By inspection, the eigenvalues are arranged along a circle, as befits the interpretation in terms of image branes. In this picture, the perturbation of line (3.7) corresponds to moving each image in or out. Similar considerations hold from analyzing the "radius squared" obtained from $\text{Tr}(Q_+^{\dagger}Q_+ + Q_-^{\dagger}Q_-)$.

In the low-energy effective field theory, the fluctuation δx signals the presence of a free chiral multiplet, which we associate with a corresponding Goldstone mode. Note that the field range of this mode is limited to small fluctuations. Indeed, as we

increase the size of δx, we can jump from one value of k to another value. In the stringy geometry, this completely changes the compactification geometry. In the low-energy effective field theory specified by the puncture, this value of k shows up in the spectrum of defect/line operators, as per reference [24]. From this perspective, we interpret possible jumping behavior in the 4D vacua as a phenomenon akin to skyrmionic excitations. We leave a complete treatment of this interesting phenomenon for future work.

3.3 Minimal momenta and maximal positions

Much as in other classical systems, it is helpful to analyze the special cases where $|p(i)|$ is as small as possible. Unlike a system with continuous time steps, however, this minimal value need not be zero. As it is helpful in characterizing other aspects of our solutions, we now study in detail the minimal momenta obtained in the orbit of an eternal puncture. The general claim we make is that in the course of its evolution, the momenta will always pass to a small value, p:

$$|p| \leq 1/2. \tag{3.10}$$

Moreover, the corresponding value of the position leads to an approximation of the maximum which would be obtained in the continuum limit of infinitesimal time steps.

To see why this always occurs, it is enough to consider the special case where $p(1) > 0$ and $x(1) > 0$. Indeed, if $p(1) < 0$ and $x(1) < 0$, the same argument will apply, and in the case where $x(1)$ and $p(1)$ have opposite sign, we observe that by evolving the system for a sufficient number of time steps, they eventually have the same sign anyway.

Consider, then, the case where $p(1) > 0$ and $x(1) > 0$. In this case, we proceed for some number of time steps until the sign of $x(i)$ changes from positive to negative. To determine where this occurs, write $p(1)$ as:

$$p(1) = p + m, \tag{3.11}$$

where $m \in \mathbb{Z}_{\geq 0}$ and $|p| \leq 1/2$. If $m = 0$, then there is nothing to show, so we assume to the contrary that $m > 0$. Now, after the first time step, the new values for our dynamical system are:

$$p(2) = p + m - \operatorname{sgn} x(1) = p + m - 1, \tag{3.12}$$

$$x(2) = x(1) + p(1) - \operatorname{sgn} x(1) = x(1) + p + m - 1, \tag{3.13}$$

so again, $x(2) > 0$. Thus, there will be a sequence of $+$ signs for $x(j)$, and eventually there will be a sign flip at some later value of j. Continuing in this way, we seek out the largest value of j such that:

$$x(j) > 0 \quad \text{for} \quad 1 \leq j \leq j_* \quad \text{and} \quad x(j_* + 1) < 0. \tag{3.14}$$

Iterating the dynamical system j times in this range, we have, by assumption, that:

$$x(j+1) = x(1) + jp(1) - \frac{j(j+1)}{2} = x(1) + j(p+m) - \frac{j(j+1)}{2}. \quad (3.15)$$

This is a quadratic polynomial in j, and its zeros occur at:

$$j_{\pm} = \left(p + m - \frac{1}{2}\right) \pm \sqrt{\left(p + m - \frac{1}{2}\right)^2 + 2x(1)}, \quad (3.16)$$

which in general is not an integer. The first integer value of j which yields a negative value, namely $x(j_{\text{flip}}) < 0$, is then given by rounding up using the ceiling function:

$$j_{\text{flip}} = \text{Ceil}\left[\left(p + m - \frac{1}{2}\right) + \sqrt{\left(p + m - \frac{1}{2}\right)^2 + 2x(1)}\right]. \quad (3.17)$$

We can also establish a crude lower bound for j_{flip} since $x(1) > 0$:

$$j_{\text{flip}} \geq 2p + 2m - 1, \quad (3.18)$$

so in other words, the integral part of $p(1)$ is bounded above by:

$$m \leq p + \frac{j_{\text{flip}} + 1}{2}. \quad (3.19)$$

Due to this, we see that $p(i)$ can indeed decrease for m steps while $x(i)$ still remains positive. At the $(m+1)$th step, the value of $p(m+1)$ and $x(m+1)$ is therefore:

$$p(m+1) = p \quad (3.20)$$

$$x(m+1) = x(1) + \frac{m^2}{2} + m\left(p - \frac{1}{2}\right). \quad (3.21)$$

We also see that this minimal value of $p(i)$ coincides with a maximal value of $x(i)$, much as one would expect in extremizing a continuous function. To see this, note first that $x(i)$ is strictly increasing as we move from $i = 1, \ldots, m+1$. Additionally, at $i = m+2$, we have that $x(m+1)$ is still positive, but that:

$$p(m+2) = p - \frac{1}{2}, \quad (3.22)$$

$$x(m+2) = x(m+1) + (p-1), \quad (3.23)$$

so $x(m+2) < x(m+1)$, since $(p-1) < 0$. See Fig. 2 for a depiction of this local maximum. Given this, it is also natural to ask where the next local extremum will

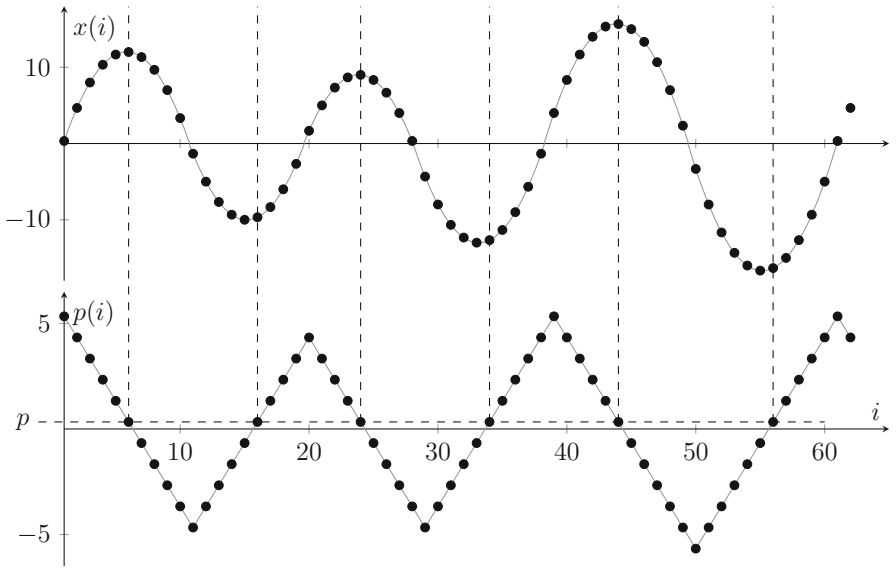

Fig. 2 Approximated maxima and minima of $x(i)$ arise for all i where $p(i) = p$ holds. In the plotted example, we have $x(1) = 1/3$, and $p(1) = x(1) + 5$, with $p = 1/3$. For this case, we realize an eternal puncture where no $x(i)$ vanishes, and the total length of the orbit is $k = 60$

occur. Indeed, after reaching the "top of the hill", we see that the $x(i)$ start to decrease until eventually we pass to a negative value of $x(j_{\text{flip}})$ where the position flips sign:

$$p(j_{\text{flip}}) = p(1) - (j_{\text{flip}} - 1), \tag{3.24}$$

$$x(j_{\text{flip}}) = x(1) + (j_{\text{flip}} - 1)p(1) - \frac{j_{\text{flip}}(j_{\text{flip}} - 1)}{2}. \tag{3.25}$$

The $x(i)$ for $i \geq j_{\text{flip}}$ then remain negative for some additional number of time steps.

Returning to our original argument, we also see that $p(j_{\text{flip}})$ can be written as:

$$p(j_{\text{flip}}) = p + \big(m - (j_{\text{flip}} - 1)\big), \tag{3.26}$$

namely the term in parentheses is a negative integer, and p is again a rational number between $-1/2$ and $+1/2$. Continuing with our previous discussion, we know that since $p(j_{\text{flip}})$ and $x(j_{\text{flip}})$ are both negative, the values of $x(i)$ will now be negative for a while and will eventually reach a minimal value for $p(i)$ where the momentum reaches its smallest norm, namely p. Letting $i_{\max}$ denote the local value of the first "maximum" where $x(i_{\max}) > 0$ and $p(i_{\max}) = p$, and $i_{\min}$ denote the first minimum where $x(i_{\min}) < 0$ and $p(i_{\min}) = p$, we see that:

$$p(i_{\min}) = p(i_{\max}) - \sum_{i_{\max} \leq j \leq i_{\min} - 1} \operatorname{sgn} x(j), \tag{3.27}$$

so in particular, since the momentum is the same at the "top of the hill" and the "bottom of the hill", namely $p(i_{\min}) = p(i_{\max}) = p$, we have an equal number of $+$ and $-$ signs for $\operatorname{sgn} x(j)$ in this range.

We can also calculate the number of time steps between each local maximum and minimum. Indeed, since we now know that the trajectory hits an equal number of $+$ and $-$ signs in passing between the two extrema, it is enough to start at $i = i_{\max}$ and evolve until the $x(i)$ flip sign. Doing so, we require the existence of a positive integer l_+ with:

$$x(l_+ + i_{\max}) > 0, \tag{3.28}$$

$$x(l_+ + i_{\max} + 1) < 0. \tag{3.29}$$

So, since we also know:

$$x(l_+ + i_{\max} + 1) = x(i_{\max}) + l_+ p(i_{\max}) - \frac{l_+(l_+ + 1)}{2}, \tag{3.30}$$

we can solve for the roots of this quadratic equation in l_+ to find the corresponding value of l_+:

$$l_+ = \text{Floor}\left[\left(p - \frac{1}{2}\right) + \sqrt{\left(p - \frac{1}{2}\right)^2 + 2x(i_{\max})}\right]. \tag{3.31}$$

Going another l_+ steps, we reach a minimum:

$$x(i_{\min}) = x(2l_+ + i_{\max} + 1) = x(i_{\max}) + 2l_+ p(i_{\max}) - \left(\frac{l_+}{2}\right)^2. \tag{3.32}$$

We can also evaluate the total length of time taken in passing from the local maximum to the local minimum:

$$i_{\min} - i_{\max} = 2\text{Ceil}\left[\left(p - \frac{1}{2}\right) + \sqrt{\left(p - \frac{1}{2}\right)^2 + 2x(i_{\max})}\right], \tag{3.33}$$

where we have used the fact that the number of $+$'s and $-$'s is exactly the same in passing from the local maximum to the local minimum. Passing now from the local minimum to the next maximum, we obtain a rather similar expression, but where we now start with $x(i_{\min}) < 0$, eventually reaching a local maximum. Labeling the local extrema as $i = i_{\text{ext}}^{(1)}, i_{\text{ext}}^{(2)}, i_{\text{ext}}^{(3)}, \ldots$, in which $i_{\text{ext}}^{(\text{odd})}$ denotes a local maximum and $i_{\text{ext}}^{(\text{even})}$ denotes a local minimum for the position $x(i)$, and the distance $l^{(m)}$ between subsequent extrema is:

$$l^{(m)} = i_{\text{ext}}^{(m+1)} - i_{\text{ext}}^{(m)} = 2\text{Ceil}\left[\left(p\operatorname{sgn} x(i_{\text{ext}}^{(m)}) - \frac{1}{2}\right) + \sqrt{\left(p\operatorname{sgn} x(i_{\text{ext}}^{(m)}) - \frac{1}{2}\right)^2 + 2\left|x(i_{\text{ext}}^{(m)})\right|}\right]. \tag{3.34}$$

Since we are ultimately interested in determining periodic orbits of the dynamical system, it is clearly fruitful to focus on this special subset of values. The evolution from one extremum to the next is again controlled by a recursion relation:

$$x(i_{\text{ext}}^{(m+1)}) = x(i_{\text{ext}}^{(m)}) + l^{(m)} p_{\min} - \left(\operatorname{sgn} x(i_{\text{ext}}^{(m)})\right) \times \left(\frac{l^{(m)}}{2}\right)^2 . \tag{3.35}$$

Rather importantly, we also see that the value of the momentum is the same for all of these special values:

$$p = p(i_{\text{ext}}^{(1)}) = p(i_{\text{ext}}^{(2)}) = \cdots . \tag{3.36}$$

To find initial conditions for which we execute a periodic orbit, it is therefore enough to find two values of extremal values for which the value of $x(i)$ repeats, namely:

$$x(j_{\text{ext}}) = x(j'_{\text{ext}}). \tag{3.37}$$

Our aim in the following subsection will be to determine the conditions necessary to achieve such a periodic orbit.

3.4 Periodic orbit conditions

We would now like to understand in greater detail the requirement that our orbit is actually periodic. The purpose of Appendix 1 is to formally prove:

$$p(1) = \frac{a}{b} \quad \text{with} \quad a, b \text{ coprime and } b \neq 0 \bmod 4 \Rightarrow \text{Periodic orbit.} \tag{3.38}$$

When $b = 0 \bmod 4$, we also find strong numerical evidence that the orbit never closes. We have explicitly checked this up to orbit lengths $k \leq 2000$.

The main element of the proof is to study what happens when the $x(i)$ become very large. Indeed, we know that for a periodic orbit there is always an upper bound on all the $x(i)$, so an orbit which is not periodic must necessarily suffer from unbounded growth in the $x(i)$. Thankfully, as $x(i)$ becomes very large, some of the non-analytic behavior in the locations of sign flips is also reduced. The main strategy of the proof presented in Appendix is that in this regime, the effects of the square root appearing in the length of a contiguous block of $+/-$'s disappear, and a simplified dynamical system involving the ceiling function is all that remains. This is still a challenging dynamical system to analyze, but the number theoretic aspects of its behavior are amenable to an exact analysis.

To see how this comes about, we first present an analytic treatment for the time evolution governed by (3.35). In order to increase the readability of the equations in this subsection, we use the abbreviations:

$$y^{(m)} = x(i_{\text{ext}}^{(m)}) \quad \text{and} \quad l = l^{(1)}. \tag{3.39}$$

In addition to the evolution $y^{(m)} \to y^{(m+1)}$ in (3.35), we also need its inverse $y^{(m)} \to y^{(m-1)}$ in the following discussion. It is given by

$$y^{(m-1)} = y^{(m)} - \tilde{l}^{(m)} p - \left(\frac{\tilde{l}^{(m)}}{2}\right)^2 \operatorname{sgn}(y^{(m)} - p) \quad \text{with} \tag{3.40}$$

$$\tilde{l}^{(m)} = 2\operatorname{Ceil}\left[-p \operatorname{sgn}(y^{(m)} - p) - \frac{1}{2} + \sqrt{\left(-p \operatorname{sgn}(y^{(m)} - p) - \frac{1}{2}\right)^2 + 2\left|y^{(m)} - p\right|}\right]. \tag{3.41}$$

Finally, note that Eqs. (3.35) and (3.34) possess a $\mathbb{Z}_2$ symmetry acting as

$$y^{(m)} \to -y^{(m)}, \quad p \to -p, \quad l^{(m)} \to l^{(m)}. \tag{3.42}$$

Therefore, it is sufficient to restrict the following discussion to $0 < p < 1/2$. From the results for positive p, the time evolution for negative p follows immediately by flipping the sign of $y^{(m)}$.

In general, it not possible to find an analytic expression for all $y^{(m)}$ starting from an arbitrary initial value $y^{(1)}$. This is due to three properties of Eqs. (3.34) and (3.35):

1. Equation (3.34) contains the highly nonlinear ceiling function
2. Equation (3.34) contains a square root
3. Equation (3.35) is nonlinear in $l^{(m)}$.

Item one captures a fundamental feature of the dynamical system. Hence, we cannot get rid of the ceiling function. But, we can deal with the two other points, if we impose some additional restrictions on $y^{(m)}$. To see how this works, we first switch from $y^{(m)}$ to the more adapted variable $\Delta^{(m)}$. It is implicitly defined as:

$$y^{(m)} = \frac{l-1}{8}\left((l-1)\operatorname{sgn} y^{(m)} + 4(\Delta^{(m)} - p)\right). \tag{3.43}$$

In terms of this new variable, (3.34) reads

$$l^{(m)} = l - \operatorname{sgn} y^{(m)} - 1 + 2\operatorname{Ceil}\left(\Delta^{(m)} + \delta_1(\Delta^{(m)}, y^{(m)})\right) \tag{3.44}$$

with

$$\delta_1(\Delta, y) = \begin{cases} \frac{1-l}{2} + p - \Delta + \frac{1}{2}\sqrt{l^2 + l(4\Delta - 4p - 2) + 4p^2 - 4\Delta + 2} & y > 0 \\ \frac{1-l}{2} - p + \Delta + \frac{1}{2}\sqrt{l^2 + l(4p - 4\Delta - 2) + 4p^2 + 4\Delta + 2} & y < 0. \end{cases} \tag{3.45}$$

In the same fashion, we rewrite (3.35) as

$$\Delta^{(m+1)} = \Delta^{(m)} + 1 + 2p - 2\operatorname{Ceil}\left(\Delta^{(m)} + \delta_1(\Delta^{(m)}, y^{(m)})\right) + \delta_2(\Delta^{(m)}, y^{(m)}) \tag{3.46}$$

with

$$\delta_2(\Delta, y) = \operatorname{sgn} y \, \frac{(1 + 4p - 2\mathrm{Ceil}(\Delta))(2\mathrm{Ceil}(\Delta) - 1)}{2(l-1)}. \tag{3.47}$$

We repeat these steps also for the inverse evolution (3.40) and (3.41) to obtain

$$\tilde{l}^{(m)} = l - \operatorname{sgn}(y^{(m)} - p) - 1 + 2\mathrm{Ceil}\left(\Delta^{(m)} - 2p + \delta_1(\Delta^{(m)}, y^{(m)} - p)\right) \tag{3.48}$$

and

$$\Delta^{(m-1)} = \Delta^{(m)} + 1 - 2p - 2\mathrm{Ceil}\left(\Delta^{(m)} - 2p + \delta_1(\Delta^{(m)}, y^{(m)} - p)\right) + \tilde{\delta}_2(\Delta^{(m)}, y^{(m)}) \tag{3.49}$$

with

$$\tilde{\delta}_2(\Delta^{(m)}, y^{(m)}) = \operatorname{sgn}(y - p) \, \frac{\Big(1 - 4p - 2\mathrm{Ceil}(\Delta - 2p)\Big)\Big(2\mathrm{Ceil}(\Delta - 2p) - 1\Big)}{2(l-1)}. \tag{3.50}$$

Note that all the results presented so far are just a mere rewriting of Eqs. (3.35), (3.34), (3.40) and (3.41). They do not involve any approximations. In this form, all contributions from the square root in (3.34) and the nonlinear parts in (3.35) are captured by the functions $\delta_1(\Delta, y)$ and $\delta_2(\Delta, y)$. The same holds for the inverse iteration. Following this observation, we implement a similar splitting for $\Delta^{(m)}$. More specifically, it splits into a leading contribution $\Delta_{\mathrm{L}}^{(m)}$ (L for leading) and corrections $\delta^{(m)}$

$$\Delta^{(m)} = \Delta_{\mathrm{L}}^{(m)} + \delta^{(m)}. \tag{3.51}$$

To make this splitting unique, we make two self-consistent definitions:

$$\delta^{(1)} \equiv -\delta_1(\Delta^{(1)}, y^{(1)}) \tag{3.52}$$

and

$$\Delta_{\mathrm{L}}^{(m+1)} \equiv \Delta_{\mathrm{L}}^{(m)} + 1 + 2p - 2\mathrm{Ceil}(\Delta_{\mathrm{L}}^{(m)}). \tag{3.53}$$

An immediate consequence of substituting Eq. (3.51) into equation (3.44) for $m = 1$ is that

$$-1 < \Delta_{\mathrm{L}}^{(1)} < 1. \tag{3.54}$$

The major advantage of the leading contribution $\Delta_{\mathrm{L}}^{(m)}$ is that the only nonlinearity it contains is the ceiling function. Thus, we can derive an analytic expression for the time evolution $\Delta_{\mathrm{L}}^{(m)}$ starting from the initial value $\Delta_{\mathrm{L}}^{(1)}$. First, we go one step further than before

$$\Delta_{\mathrm{L}}^{(m+2)} = \Delta_{\mathrm{L}}^{(m)} + 4p + 2\mathrm{Ceil}(\Delta_{\mathrm{L}}^{(m)}) - 2\mathrm{Ceil}(\Delta_{\mathrm{L}}^{(m)} + 2p). \tag{3.55}$$

Applying this equation multiple times implies

$$\Delta_{\mathrm{L}}^{(m+2n)} = \Delta_{\mathrm{L}}^{(m)} + 4np + 2\sum_{l=0}^{2n-1}(-1)^l \,\mathrm{Ceil}(\Delta_{\mathrm{L}}^{(m)} + 2lp). \tag{3.56}$$

Here, then, is the crux of the analysis: Although we started with a highly nonlinear dynamical system with both a square root function and a ceiling function, the reduced evolution equation as captured by Eq. (3.56) only involves integral quantities. As such, it is easier to analyze the periodic behavior of this system. In particular, we can already anticipate that there is something special about the value of b mod 4 in the ratio $p = a/b$ because of the factors of 4 appearing in Eq. (3.56). The caveat to this is of course that the "rounding errors" that we make at each stage of our evolution equation remain bounded and small. One of the purposes of Appendix 1 is to establish this property in the special limit where the initial value $x(1)$ is sufficiently large (as measured in units of b).

Qualitatively, we also understand from Lemma 2 in Appendix 1 why orbits with b mod 4 do not close (even if we do not give a formal proof by analyzing all the rounding errors explicitly). This lemma states that after $b/2$ extrema, the dominant contribution $\Delta_{\mathrm{L}}^{(m)}$ increases by one:

$$\Delta_{\mathrm{L}}^{(m+b/2)} = \Delta_{\mathrm{L}}^{(m)} + 1. \tag{3.57}$$

Neglecting the subleading corrections, this results implies that the length of contiguous blocks of $+/-$ grows over time and therewith $|x(i_{\min})|/|x(i_{\max})|$. Figure 3 demonstrates this effect for $p(1) = 5/4$ and $x(1) = 1/4$.

Another by-product of our analysis is that when $x(1)$ is sufficiently large and we have a periodic orbit, we have a "dominant orbit," namely the leading-order contribution completely captures the evolution of the dynamical system, and all rounding errors remain small. For such dominant orbits, we can even obtain an analytic formula for the value of k, the length of the orbit:

$$k = l^{(*)}k' + 2k'p, \tag{3.58}$$

where $l^{(*)}$ is a particular choice of $l^{(m)}$, as defined in Eq. (3.34), and k' is the number of extrema in the orbit. The particular value of m which enters here is the one for which:

$$0 < \mathrm{sgn}(y^{(m)})\Delta_{\mathrm{L}}^{(m)} < \frac{1}{k'}. \tag{3.59}$$

4 Terminal punctures

Having understood some of the general properties of eternal punctures, we now turn to the structure of the dynamical system in the case of terminal punctures. In this case, it can happen that the full description of the puncture will decompose into several

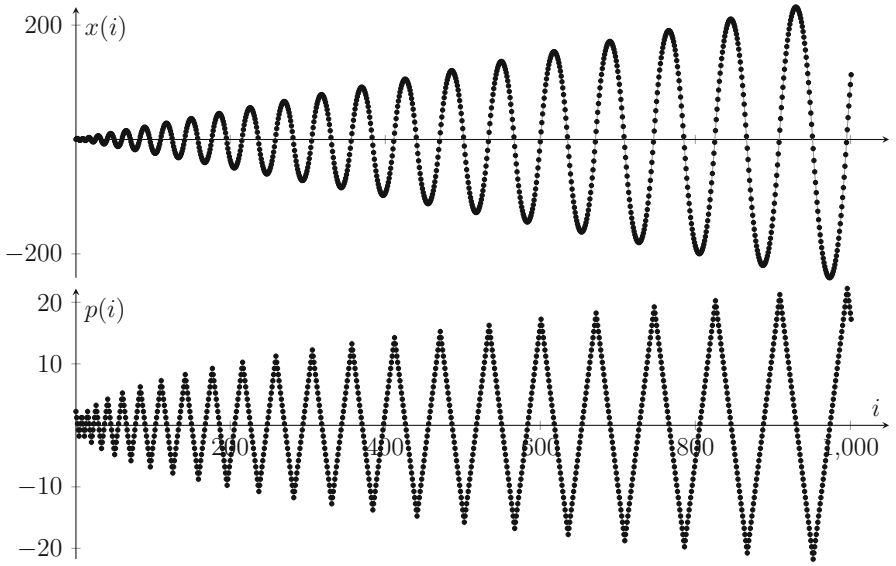

Fig. 3 A generic feature of initial conditions with $p = a/b$ and $b \bmod 4 = 0$ is that the enveloping curves of $x(i)$ and $p(i)$ grow over time. Therefore, all examples we have studied numerically do not seem to close into a periodic orbit. Here, this feature is depicted for the initial conditions $p(1) = 5/4$, $x(1) = 1/4$ and the first 1000 $x(i)/p(i)$ of the time evolution

independent pieces, because at each termination point, we can restart at the next time step with a new choice of initial condition.

With this in mind, we consider a puncture for which $x(0) = x(k) = 0$. Given some choice of initial conditions, we would like to track the subsequent evolution under Eq. (2.18):

$$\begin{bmatrix} p(i+1) \\ x(i+1) \end{bmatrix} = \begin{bmatrix} 1 & 0 \\ 1 & 1 \end{bmatrix} \begin{bmatrix} p(i) \\ x(i) \end{bmatrix} - \begin{bmatrix} \operatorname{sgn} x(i) \\ \operatorname{sgn} x(i) \end{bmatrix}. \tag{4.1}$$

To begin, we have the necessary condition:

$$x(1) = p(1) = p(0), \tag{4.2}$$

so in some sense, everything is dictated by the choice of a single real parameter, $p(0)$. Remarkably, the late-time behavior of the dynamical system turns out to be quite sensitive to this initial condition.

Our next task is to understand which values of this initial condition can produce a terminal puncture. Along these lines, we observe that upon solving for the $p(i)$ and $x(i)$, we can iterate until for some $i = i_*^{(1)}$, $x(i_*^{(1)}) = 0$. Note that by assumption that we have a non-trivial terminal puncture, this occurs for $2 \leq i_1^* \leq k$. Since this also means $x(i)$ is nonzero for these intermediate values, the puncture equations and the dynamical system lead to the same conditions on the $x(i)$ and $p(i)$. Iteratively solving for the $x(i)$, we then obtain the necessary conditions summarized by the matrix equation:

$$\begin{bmatrix} 2 & -1 & & & \\ -1 & 2 & -1 & & \\ & -1 & \ddots & -1 & \\ & & -1 & 2 & -1 \\ & & & -1 & 2 \end{bmatrix} \begin{bmatrix} x(1) \\ x(2) \\ \vdots \\ x(k-2) \\ x(i_*^{(1)}-1) \end{bmatrix} = \begin{bmatrix} \operatorname{sgn} x(1) \\ \operatorname{sgn} x(2) \\ \vdots \\ \operatorname{sgn} x(i_*^{(1)}-2) \\ \operatorname{sgn} x(i_*^{(1)}-1) \end{bmatrix}, \tag{4.3}$$

where the $(i_1^*-1)\times(i_1^*-1)$ matrix is the Cartan matrix for an A-type root system, in the obvious notation. Inverting the Cartan matrix, we see that all of the $x(i)$ are necessarily rational numbers, so we must require our initial condition $p(0)$ to be a rational number, which we write as:

$$p(0) = p(1) = x(1) = \frac{a(1)}{b} \quad \text{for } a(1), b \text{ relatively prime.} \tag{4.4}$$

In the context of the dynamical system, nothing stops us from continuing to evolve our values of the $x(i)$. As we have already remarked, a "short orbit" is one for which $x(i_*^{(1)}+1) = x(1)$, whereas for a "long orbit" we must instead cycle around once more before we repeat back to $x(1)$. In the context of finding punctures, of course, there is no need to continue evolving with the dynamical system once we reach a termination point. Indeed, we are free to restart the dynamical system with some other choice of initial conditions, in which case we obtain a terminal puncture with multiple irreducible components.

We observe that we can pass from a terminal puncture back to an eternal puncture by making a sufficiently small perturbation in the value of $x(1)$, namely:

$$x(1) \mapsto x(1) + \delta x. \tag{4.5}$$

If the terminal puncture yields a periodic orbit, it follows that the system with the perturbed initial condition will also yield a periodic orbit. Indeed, this is the key feature of having a small continuous parameter in the eternal punctures.

But for the eternal punctures, we already argued that to reach a periodic orbit, a necessary and sufficient condition is that $p(1) = a(1)/b$ with $b \neq 0 \bmod 4$. So, we see that this condition also holds for terminal punctures:

$$\text{Terminal puncture: } p(1) = x(1) = \frac{a(1)}{b} \quad \text{with } b \neq \bmod 4. \tag{4.6}$$

We reach these special orbits by appropriate tuning of the parameter δx.

Now, from the perspective of the puncture equations, we can equally well characterize the evolution by the values of $x(i)$, or by simply stating the sequence of signs that are obtained from a particular choice of initial condition. As we change the value of the initial condition, however, this sequence will bifurcate to two distinct sequences, and can then bifurcate further after some further number of time steps. Of course, the delicate part in the analysis is that a priori, we do not know which of the 2^k possible sequences will actually yield a solution to the puncture equations.

Let us give a few examples to illustrate the general idea. For $p(0) = p(1) = k/2$, we find that $\mathrm{sgn}(x(i)) = +1$ for $1 \leq i \leq k$. Moreover, the parent matrix $\widetilde{Q} = 0$, so we generate a representation of $\mathfrak{su}(2)$. Indeed, the eigenvalues of the generator of the Cartan subalgebra in such a representation are always half integers or integers, so this is not particularly surprising. Note also that if $p(1) = a(1)/b$ has b different from 1 or 2, we necessarily do not have a representation of $\mathfrak{su}(2)$.

A non-trivial class of examples in which the signs alternate occurs when $k = 2n$ is even:

$$l = \frac{n}{2n+1} \Rightarrow \{\mathrm{sgn}\, x(i)\}_{i=1}^{k} = \underbrace{+, -, \ldots, +, -}_{2n}. \tag{4.7}$$

To determine viable sequences of signs, we therefore use a standard tool in dynamical systems: We consider without loss of generality the value of the parameter l and seek out bifurcation points where the sign of $x(i)$ is about to split. These special bifurcation points tell us the locations of finite length periodic orbits. Iterating in this way, we can determine both the initial condition and the corresponding value of k appearing in the puncture equations.

Applying the evolution Eq. (4.1) on the interval $[0, \infty)$, this line segment splits into two segments specified by the conditions $x(2) < 0$ and $x(2) > 0$. The bifurcation point amounts to splitting the interval up into two subintervals for possible values of the initial condition, namely $0 \leq p(0) < 1/2$ and $1/2 < p(0) < \infty$. By repeating this procedure, one finds more and more new line segments and the partition of the parameter interval for $p(0)$ gets finer. Figure 4 depicts this process for the first three iterations. In the upper left corner, there is the initial line segment $[0, \infty)$ which is completely in the right quadrant with $x > 0$. In order to iterate this segment, we apply the evolution Eq. (4.1) to each of its points and so obtain the diagram for $i = 2$ on the upper right. Moreover, we split the line segment into two parts so that each one only has points in one quadrant either $x > 0$ or $x < 0$. After iterating and splitting them again, one arrives at the diagram for $i = 3$ in the lower left corner. So far the number of line segments has grown exponentially as a function of k. This drastically changes starting with the fourth iteration, resulting in the last diagram of Fig. 4. Here, only one of the four line segments arising by iteration from the last step is located in two quadrants and therefore needs splitting. Of course, we can also identify the various segments in this diagram with the following intervals:

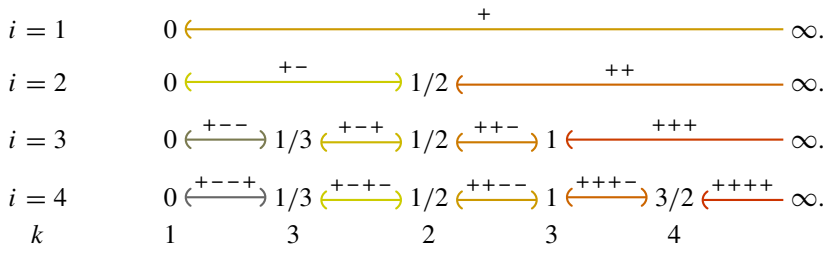

(4.8)

of the parameter $p(1)$ where we use the same color coding as in Fig. 4. Additionally, the signs + and − denote the quadrants ($x(i) > 0$ and $x(i) < 0$) which these segments

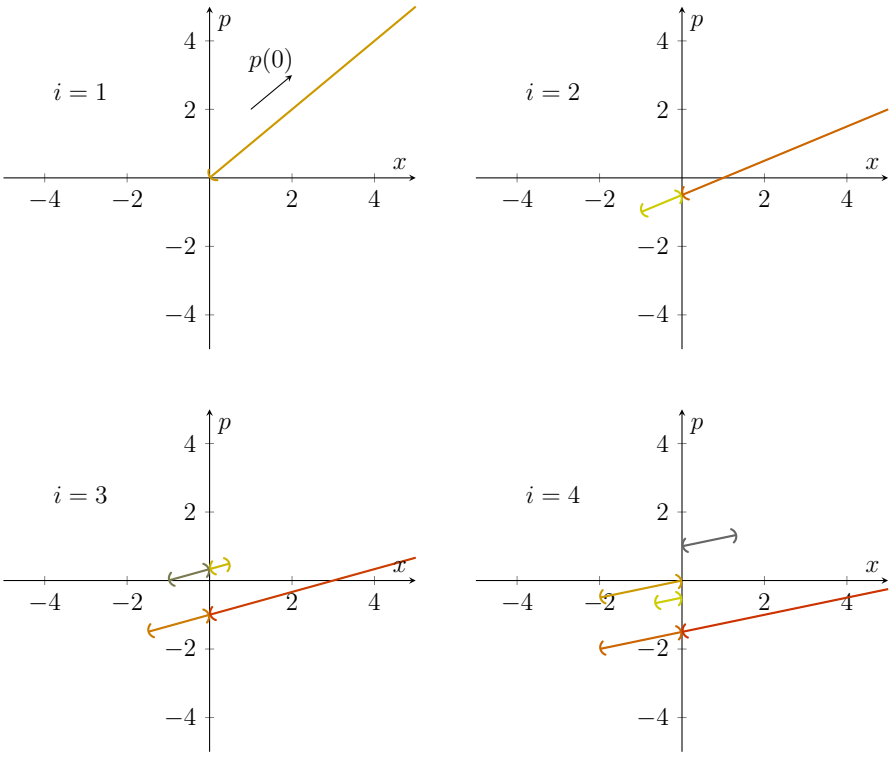

Fig. 4 Three iterations of the initial line segment $[0, \infty)$ which give rise to bifurcating behavior in the initial condition l (color figure online)

are in after the ith iterations. They are read from left to right. It is obvious that the first one is always $+$, because the initial interval is completely in the quadrant $x(1) > 0$. Doing further iterations, result in a refinement of this diagram. There are a few initial conditions $l \in \{1/3, 1/2, 1, 3/2\}$ which we excluded so far. They give rise to the four smallest periodic orbits of the dynamical system. Their length k is equivalent to the value of i where the value of l appears as a interval boundary for the first time. For a depiction of the branching, see Fig. 5.

4.1 Irreducible representations

Though the dynamical system is clearly quite sensitive to initial condition data, it nevertheless exhibits some regular features, at least for certain values of the orbit length k. To track this behavior, we first list out m_k, the number of terminal punctures with length k and $x(k) = 0$, with no vanishing of any $x(i)$ for $0 < i < k$. The multiplicity of these "irreducible representations" for small values of k is as follows:

$$\begin{array}{cccccccccccccccccccc} k & 2 & 3 & 4 & 5 & 6 & 7 & 8 & 9 & 10 & 11 & 12 & 13 & 14 & 15 & 16 & 17 & 18 & 19 & 20 \\ m_k & 2 & 4 & 2 & 6 & 6 & 8 & 2 & 12 & 10 & 12 & 6 & 14 & 14 & 22 & 2 & 18 & 18 & 20 & 10. \end{array} \tag{4.9}$$

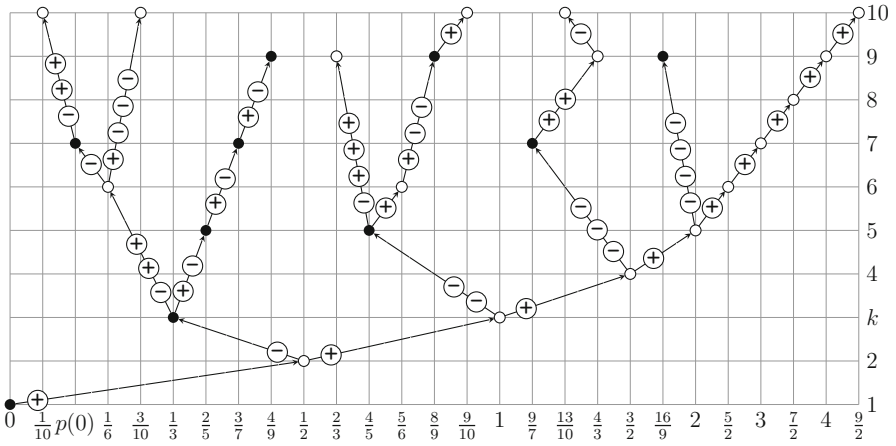

Fig. 5 Periodic orbits which represent the 1/2 BPS punctures of the A_k theory for $k \leq 10$ if one link between the quiver nodes is turned off. Whether a node is filled or not distinguishes between short and long orbits. Each link between two nodes carries the sequence of $\mathrm{sgn}x(i)$ which has to be appended to the shorter orbit in order to obtain the longer one

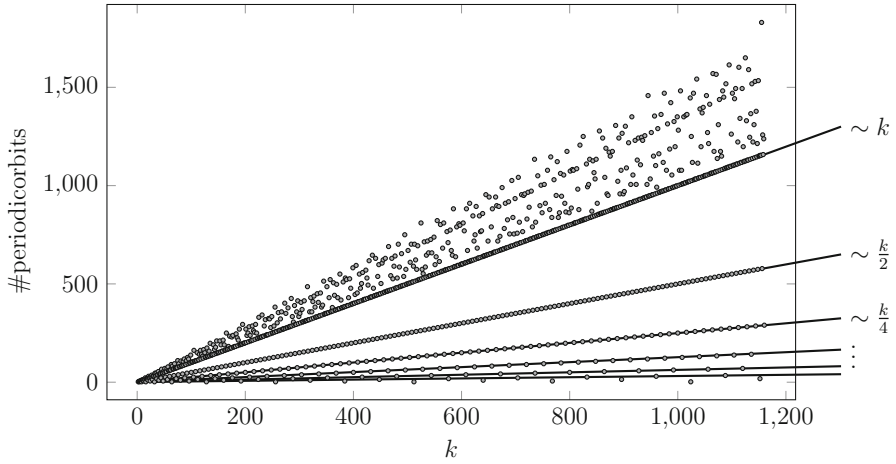

Fig. 6 Number of periodic orbits with the length k. The regular subsequences are marked by lines with slope $k/2^j$

This sequence contains some regular subsequences as can already be seen from the first contributions but becomes more obvious by looking at a larger number of k as depicted in Fig. 6.

Some of the multiplicities satisfy rather regular patterns. For example, we have:

$$m_{k_j(n)} = 4n - 2 \quad \text{for all} \quad j \in \mathbb{N} \quad \text{with} \quad k_j(n) = 2^j(2n-1). \tag{4.10}$$

All solutions belonging to these subsequences are long orbits. In total, this regular contribution fixes half of the sequence m_k, namely for k even. This also explains why

it only contains long orbits. Short orbits require k to be odd. For odd k, there seems to be no regular pattern, as shown in Fig. 6.

5 Higher-order poles

Having presented a general characterization of simple poles, we now turn to the structure of punctures with higher-order poles. As we have already remarked in Sect. 2, the structure of the first-order pole involves nonlinear quadratic evolution in the values of the q and $\widetilde{q}$'s. At second order and above, however, the structure becomes linear in these parameters, since the lower-order poles essentially serve as "boundary conditions" for evolution in the pole order. It thus follows that as we evolve from one pole order to the next, there is sometimes a degree of freedom associated with whether we continue to higher order, but for the most part, all of this is fully fixed by the lower-order terms. This holds for general values of k and N in our puncture equations. Here, we only study the $N = 1$ case explicitly for which we have full control over the first order. With this in mind, we assume that we have been given a consistent solution $q_1(i)$, $\tilde{q}_1(i)$ and $p_1(i)$, and then deduce the structure of the higher-order poles for this puncture. Indeed, for "generic" choices of initial conditions at lower order, we can evolve to a higher-order solution. There are, however, possible obstructions to continuing this evolution indefinitely to higher-order poles, and part of our aim in this section will be to determine these obstructions. Modulo this caveat, however, we see a sharp sense in which the dynamical system involves evolution in "time" (namely from one quiver node to its neighbor) and "space" (namely from one pole order to the next).

For the higher-order contributions $\Sigma_m(i)$, $Q_m(i)$ and $\tilde{Q}_m(i)$, we use the same parameterization as for the leading ones in (2.6)–(2.8). It is convenient to combine these data to a vector

$$\vec{v}_m(i) = \left[q_m(i)\ \tilde{q}_m(i)\ p_m(i)\right] \tag{5.1}$$

for every node of the A-type quiver. The constraint Eq. (2.2) give rise to a system of affine maps system of affine maps which connect the puncture data along the quiver. We split this system into a linear part $M_m(i)$ plus the offset contribution $\vec{n}_m(i)$. It gives rise to the iteration prescription

$$\vec{v}_m(i+1) = M_m(i)\vec{v}_m(i) + \vec{n}_m(i) \tag{5.2}$$

for the puncture data at level m. Assuming that we can invert and solve the first-order pole equations, the explicit expressions for $M_m(i)$ and $\vec{n}_m(i)$ follow after some algebra directly from (2.2)

$$M_m(i) = \begin{cases} \begin{bmatrix} -\alpha_m(i) + \beta_m(i) & 0 & \delta_m(i) \\ 0 & \beta_m(i) & 0 \\ -\gamma_m & 0 & 1 \end{bmatrix} & \text{for } x(i) > 0 \text{ and } x(i+1) > 0 \\ \begin{bmatrix} 0 & \beta_m(i) & 0 \\ \alpha_m(i) - \beta_m(i) & 0 & -\delta_m(i) \\ -\gamma_m(i) & 0 & 1 \end{bmatrix} & \text{for } x(i) > 0 \text{ and } x(i+1) < 0 \\ \begin{bmatrix} 0 & \alpha_m(i) - \beta_m(i) & \delta_m(i) \\ \beta_m(i) & 0 & 0 \\ 0 & \gamma_m(i) & 1 \end{bmatrix} & \text{for } x(i) < 0 \text{ and } x(i+1) > 0 \\ \begin{bmatrix} \beta_m(i) & 0 & 0 \\ 0 & -\alpha_m(i) + \beta_m(i) & -\delta_m(i) \\ 0 & \gamma_m(i) & 1 \end{bmatrix} & \text{for } x(i) < 0 \text{ and } x(i+1) < 0 \end{cases} \tag{5.3}$$

and

$$\vec{n}_m(i) = \begin{cases} \begin{bmatrix} \gamma'_m(i) + \alpha'_m(i)\delta_m(i) & \beta'_m(i) & \alpha'_m(i) \end{bmatrix}^T & \text{for } x(i) > 0 \text{ and } x(i+1) > 0 \\ \begin{bmatrix} \beta'_m(i) - \gamma'_m(i) - \alpha'_m(i)\delta_m(i) & \alpha'_m(i) \end{bmatrix}^T & \text{for } x(i) > 0 \text{ and } x(i+1) < 0 \\ \begin{bmatrix} \gamma'_m(i) - \tilde{\alpha}'_m(i)\delta_m(i) & \beta'_m(i) & -\tilde{\alpha}'_m(i) \end{bmatrix}^T & \text{for } x(i) > 0 \text{ and } x(i+1) < 0 \\ \begin{bmatrix} \beta'_m(i) & -\gamma'_m(i) + \tilde{\alpha}'_m(i)\delta_m(i) & -\tilde{\alpha}'_m(i) \end{bmatrix}^T & \text{for } x(i) > 0 \text{ and } x(i+1) < 0. \end{cases} \tag{5.4}$$

In order to write them in a compact form, the abbreviations

$$\alpha_m(i) = \gamma_m(i)\delta_m(i), \quad \beta_m(i) = \sqrt{\left|\frac{x(i)}{x(i+1)}\right|}, \quad \gamma_m(i) = \frac{m-2}{\sqrt{|x(i)|}},$$
$$\delta_m(i) = \frac{m-1}{2\sqrt{|x(i+1)|}}$$

and

$$\alpha'_m(i) = \frac{a_m(i)}{\sqrt{x(i)}}, \quad \tilde{\alpha}'_m(i) = \frac{\tilde{a}_m(i)}{\sqrt{x(i)}}, \quad \beta'_m(i) = -\frac{b_m(i)}{\sqrt{|x(i+1)|}},$$
$$\gamma'_m(i) = \frac{c_m(i+1)}{2\sqrt{|x(i+1)|}}$$

are convenient. For the next-to-leading-order contribution $m = 3$, the offset part $\vec{n}_m(i) = 0$ vanishes and we only have to take into account $M_m(i)$. Once an initial value $\vec{v}_n(1)$ is chosen, (5.2) allows to calculate all remaining $\vec{v}_n(i)$ iteratively. Hence, we only have to specify an appropriate initial value. To this end, we employ the monodromy

$$\mathbf{M}_m = M_m(k) M_m(k-1) \dots M_m(1) \tag{5.5}$$

which has to fulfill

$$\vec{v}_3(k+1) = \mathbf{M}_3 \vec{v}_3(1) = \vec{v}_3(1) \tag{5.6}$$

to be compatible with the periodic boundary conditions of the quiver. Note that $\mathbf{M}_m$ is an element of $SL(3,\mathbb{C})$. This property is based on the determinant of $M_m(i)$

$$\det M_m(i) = \beta_m(i)^2 = \frac{|x(i)|}{|x(i+1)|}, \tag{5.7}$$

which gives immediately rise to

$$\det \mathbf{M}_m = \prod_{i=1}^{k} \frac{|x(i)|}{|x(i+1)|} = \frac{|x(1)|}{|x(k+1)|} = 1. \tag{5.8}$$

However, not every eigenvector of $\mathbf{M}_3$ with eigenvalue 1 is a valid initial condition. There is the additional constraint

$$\tilde{q}_{m-1}(i) = \frac{\tilde{a}_m(i)}{m} \quad (x(1) > 0) \qquad \text{or} \quad q_{m-1}(i) = \frac{a_m(i)}{m} \quad (x(1) < 0) \tag{5.9}$$

depending whether $x(1)$ is positive or negative. It also follows from (2.2) and is preserved under the iteration prescription (5.2). Thus, the non-trivial part of the monodromy is reduced from $SL(3,\mathbb{C})$ to $SL(2,\mathbb{C})$ and a fixed point which respects (5.9) can only arise if $\mathrm{Tr}\mathbf{M}_3 = 3$ holds. This is because one eigenvalue of $\mathbf{M}_3$ has to be 1 due to (5.9). Furthermore, the two remaining eigenvalues, λ_1 and λ_2, are either complex or real. If they are complex, $\lambda_2 = \lambda_1^\dagger$ has to hold because $\mathbf{M}_3$ is real. Additionally, we find

$$\lambda_1 \lambda_2 = 1 \quad \text{and therefore} \quad \lambda_1 = \frac{1}{\lambda_2} \tag{5.10}$$

as it is required for $\det \mathbf{M}_3 = 1$. We cannot directly use the complex eigenvalues, because their eigenvalues are necessary complex too but $\vec{v}_3(1)$ has to be real. Still, we are able to assign $\vec{v}_3(1)$ to the sum of the two eigenvectors. Like their eigenvalues, they are complex conjugated to each other and so their sum is real. In order to obtain a fix point, this ansatz requires $\lambda_1 + \lambda_2 = 2$, which implies $\mathrm{tr}\,\mathbf{M}_3 = 3$. In this case, there is exactly one fixed point. It is unique up to a rescaling. For real eigenvalues, at least λ_1 or λ_2 has to be one. Otherwise there is no fixed point. But in this case, all eigenvalues are one and $\mathbf{M}_3$ is the identity matrix 1_3. As a consequence, $\vec{v}_3(1)$ is not restricted at all. Rescaling of $\vec{v}_3(1)$ has a very natural interpretation in terms of constraints (2.2). They are invariant under the transformation

$$Q_m \to \lambda^{m-1} Q_m, \quad \tilde{Q}_m \to \lambda^{m-1} Q_m \quad \text{and} \quad \Sigma_m \to \lambda^{m-1} \Sigma_m \tag{5.11}$$

with some $\lambda \in \mathbb{R}_+$ which is equivalent to $\vec{v}_3(1) \to \lambda \vec{v}_3(1)$. So without loss of generality, we fix $\|\vec{v}_3(1)\| = \sqrt{q_3^2(1) + \tilde{q}_3^2(1) + p_3^2(1)} = 1$.

If we go beyond m=3, there is also an offset contribution

$$\vec{\mathbf{n}}_m = \vec{n}_m(k) + M_m(k)\vec{n}_m(k-1) + \cdots + M_m(k)\ldots M_m(2)\vec{n}_m(1) \tag{5.12}$$

to the fixed point equation

$$\mathbf{M}_m \vec{v}_m(1) + \vec{\mathbf{n}}_m = v_m(1). \tag{5.13}$$

By taking into account the constraints on the initial conditions (5.9), this equation is again reduced to a two-dimensional subspace. Let us assume that $\vec{\mathbf{n}}_m$ does not vanish. Otherwise, the discussion for the $m = 3$ case applies without any modification. We already have noticed that for $\mathrm{tr}\,\mathbf{M}_m = 3$, the matrix $\mathbf{M}_m - 1_3$ does not have full rank. Most severe is this situation if $\mathbf{M}_m = 1_3$. In this case (5.13) does not admit a solution at all. Alternatively, $\vec{\mathbf{n}}_m$ could be in the one-dimensional image of $\mathbf{M}_m - 1_3$. Then, there is a one-dimensional family of fixed points. It is well-known from linear algebra that this family is the superposition of an inhomogeneous part and all homogeneous contributions. Latter also give rise to the dimension of the solution space. They live in the kernel of $\mathbf{M}_m - 1_3$ which is one dimensional for $\mathrm{tr}\,\mathbf{M}_m = 3$ and $\mathbf{M}_m \neq 1_3$ after removing the direction constrained by (5.9). Finally, if $\mathrm{tr}\,\mathbf{M}_m \neq 3, \mathbf{M}_m - 1_3$ is invertible and gives rise to a unique solution. All these different cases can be summarized in the decision tree

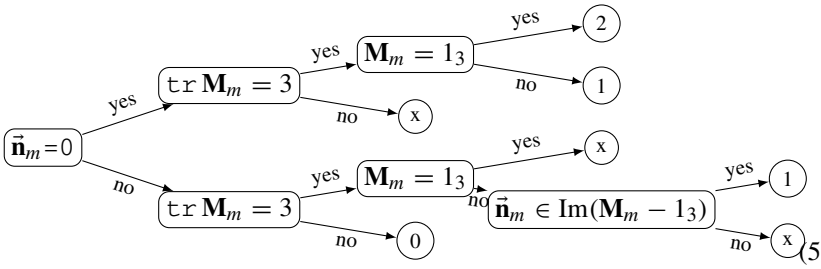

(5.14)

Here, the number in the circle denotes the dimension of the solution space, while x represents no solution at all.

In the generic case, $\mathrm{tr}\,\mathbf{M}_3 = 3$, $\mathbf{M}_3 \neq 1_3$ and $\mathrm{tr}\mathbf{M}_m \neq 3$, for all other $m > 3$. Then, the solution of the first-order problem fixes all higher orders completely. Note that it is always possible to set all $Q_m(i)$, $\tilde{Q}_m(i)$ and $\Sigma_m(i)$ to zero for all m larger or equal to n. We call such solutions n-trivial. For the generic case, there exist 3-trivial solution and a 4-trivial solution, and it goes on toward an ∞-trivial solution. In the special case, where one hits the node x for a fixed m, there are only 3-, ... m-trivial solutions.

Finally, there are some special points where additional degrees of freedom occur. Identifying them requires to evaluate the trace of the monodromy $\mathbf{M}_m$ for a family of periodic orbits with $x(k) \neq 0$. It is instructive to study a simple example to present the relevant steps. Take the initial conditions $4/5 \leq x(1) = x \leq 1$ and $p(1) = 3/2$. They give rise to a periodic orbits of length $k = 6$ and

i	1	2	3	4	5	6
$x(i)$	x	$x+1/2$	x	$x-3/2$	$x-2$	$x-3/2$
$p(i)$	$3/2$	$1/2$	$-1/2$	$-3/2$	$-1/2$	$1/2$.

(5.15)

Now, we calculate

$$\operatorname{tr}\mathbf{M}_3 - 3 = \sum_{n=0}^{12} c_n(x) m^n, \tag{5.16}$$

which is a polynomial in m with coefficients depending on x. There is no simply analytic expression for these coefficients. Still we can calculate them numerically without much effort. The same is true for the zeros m_i of the polynomial. For every value of x in the given interval, they include 3. Hence, we can always construct a non-trivial next to leading order. Moreover, there is a distinguished value of x in the interval where 4 is another integer zero. A numerical analysis shows that this value is $x = 0.88055824$. It gives rise to a family of $m = 4$ solutions with one free parameter.

6 Comments on the higher-rank case

Much of our focus up to this point has been on the relatively "simple" case of $N = 1$, but arbitrary k. From the perspective of 6D SCFTs, these punctures are most directly associated with the theory of a single M5-brane probing the transverse geometry $\mathbb{R}_\perp \times \mathbb{C}^2/\mathbb{Z}_k$. Of course, given our full characterization of the $N = 1$ and general k case, we can now produce additional solutions to the puncture equations for N M5-branes probing a general ADE singularity, as well as new 1/4 BPS punctures of class $\mathcal{S}$ theories. For the class $\mathcal{S}_\Gamma$ theories, we follow a similar procedure to that given in reference [40], namely we pick independent one-dimensional linear subspaces associated with each quiver node, and draw independent paths which connect to each such subspace. In reference [40], this was used to produce $\mathfrak{su}(2)^{\mathcal{P}}$ representations, where $\mathcal{P}$ denotes the number of independent paths. In that context, the sign of all of the $x(i)$ of a given path is fixed to all be the same, namely we obtain a directed path. From the present perspective, we can now alter the relative signs of these segments to obtain a far broader class of solutions. In particular, we are guaranteed that these are new solutions, since as we have already remarked, each such path cannot correspond to a representation of $\mathfrak{su}(2)$. See Fig. 7 for a depiction of one such undirected path for a D-type affine quiver.

It is also natural to consider particular small values of k, such as $k = 2$, but with N arbitrary. Solving the puncture equations in this case seems to be a problem of similar difficulty to simply specifying all 1/4 BPS punctures of class $\mathcal{S}$ theories. With this in mind, it seems more fruitful to see what we can say about the general structure of solutions as a function of N and k.

Indeed, more ambitiously, one might also hope to recast the general rank N case in terms of a perhaps more involved dynamical system now involving matrices. Our plan in the remainder of this section will be to show how this can at least be formally stated, though we defer the corresponding analysis of consistent initial conditions to future work.

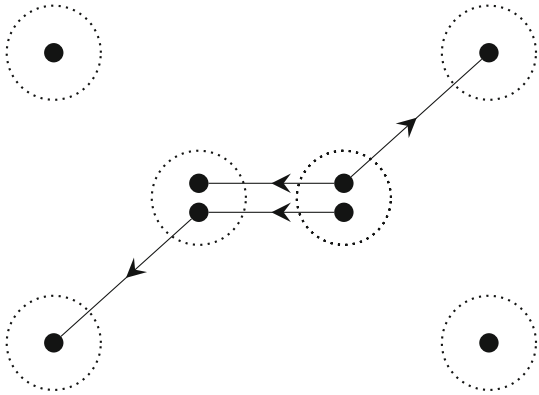

Fig. 7 Demonstration of the undirected path approach for a simple D-type quiver

To this end, we first repackage the puncture equations for the class $\mathcal{S}_k$ theories in terms of a recursion relation. Suppose, then, that we have specific values of $q(i)$, $\widetilde{q}(i)$ and $p(i)$, which, respectively, denote position and momenta in the system. In the generic case, the doublet:

$$\begin{bmatrix} q(i) \\ \widetilde{q}^{\dagger}(i) \end{bmatrix} \tag{6.1}$$

is a rank N matrix. In fact, we can see that the generic linear combination of the form:

$$\widehat{q}_{\varepsilon}(i) \equiv q(i) + \varepsilon \widetilde{q}^{\dagger}(i) \tag{6.2}$$

is invertible. One way to establish this is to work in a basis where all $p(i)$ are diagonal. In this basis, we observe that the matrix entries for the puncture equations include the constraints:

$$[p_A(i) - p_B(i+1)]\, q_{AB}(i) = q_{AB}(i) \tag{6.3}$$

$$[p_A(i) - p_B(i+1)]\, \widetilde{q}^{\dagger}_{AB}(i) = -\widetilde{q}^{\dagger}_{AB}(i), \tag{6.4}$$

so the matrix entries $q_{AB}(i)$ and $\widetilde{q}^{\dagger}_{AB}(i)$ cannot simultaneously be nonzero. For generic values of the parameter ε, we then see that both $\widehat{q}_{\varepsilon}(i)$ and $\widehat{q}_{-\varepsilon}(i)$ are invertible. Assuming this is the case, we can now solve for the next value of $p(i+1)$ in terms of the previous time step:

$$p(i+1) = \widehat{q}_{\varepsilon}^{-1}(i)\, p(i)\, \widehat{q}_{\varepsilon}(i) - \widehat{q}_{\varepsilon}^{-1}(i)\, \widehat{q}_{-\varepsilon}(i). \tag{6.5}$$

By the same token, we can also evaluate the new value of the "norm" $q(i+1)q^{\dagger}(i+1) - \widetilde{q}^{\dagger}(i+1)\widetilde{q}(i+1)$:

$$q(i+1)q^{\dagger}(i+1) - \widetilde{q}^{\dagger}(i+1)\widetilde{q}(i+1) = p(i+1) + q^{\dagger}(i)q(i) - \widetilde{q}(i)\widetilde{q}^{\dagger}(i). \tag{6.6}$$

To cast this in the form of a more explicit recursion relation, it is helpful to work in terms of the polar decomposition for the matrices q and $\widetilde{q}$. For a complex matrix $q(i)$,

this amounts to introducing a unitary matrix $W(i)$ (complex phases) and a positive definite matrix $R(i)$ (the norm) so that:

$$q(i) = R(i)W(i), \quad \widetilde{q}(i) = \widetilde{W}(i)\widetilde{R}(i), \tag{6.7}$$

where we have also introduced a similar relation for $\widetilde{q}(i)$. In terms of these matrices, the recursion relations read as:

$$p(i+1) = \widehat{q}_\varepsilon^{-1}(i)p(i)\widehat{q}_\varepsilon(i) - \widehat{q}_\varepsilon^{-1}(i)\widehat{q}_{-\varepsilon}(i), \tag{6.8}$$

$$R^2(i+1) - \widetilde{R}^2(i+1) = p(i+1) + W^\dagger(i)R^2(i)W(i) - \widetilde{W}(i)\widetilde{R}^2(i)\widetilde{W}^\dagger(i). \tag{6.9}$$

So, provided we know R, W, $\widetilde{R}$ and $\widetilde{W}$ at a given time step, we can feed this in and solve for the next time step. In practice, of course, this is still a rather involved procedure, but in principle it shows that a dynamical system continues to persist for all N.

Note that the recursion relation requires an additional input whenever we cannot solve the system, i.e., when $\widehat{q}_\varepsilon$ does not possess an inverse, and this is the higher-rank analog of having a terminal puncture in the $N = 1$ case.

It is also instructive to consider the evolution of the "center of mass" degree of freedom for the system. Taking the trace and dividing by N, we obtain:

$$\frac{1}{N}\mathrm{Tr}\left[R^2(i+1) - \widetilde{R}^2(i+1)\right] = \frac{1}{N}\mathrm{Tr}\left[p(i+1)\right] + \frac{1}{N}\mathrm{Tr}\left[R^2(i) - \widetilde{R}^2(i)\right], \tag{6.10}$$

$$\frac{1}{N}\mathrm{Tr}\left[p(i+1)\right] = \frac{1}{N}\mathrm{Tr}\left[p(i)\right] - \frac{1}{N}\mathrm{Tr}\left[\widehat{q}_\varepsilon^{-1}(i)\widehat{q}_{-\varepsilon}(i)\right]. \tag{6.11}$$

This is not quite a closed system, because the second term on the right-hand side of line (6.11) is a number between -1 and $+1$. Said differently, we need to include the higher-order matrix powers to fully fix this parameter. Note, however, that at large N, this last term can approximate an arbitrary real number in the interval $[-1, +1]$, so in this sense the jumps in the momenta can become quite small and uniform. At small N, however, the system is highly discretized, and the jumps in momenta are clearly more pronounced.

7 Conclusions

One of the important pieces of defining data for compactifications of 6D SCFTs on Riemann surfaces involves the choice of boundary data at marked points. In this work, we have classified the structure of punctures in perhaps the simplest case of a single M5-brane probing a $\mathbb{C}^2/\mathbb{Z}_k$ singularity. Starting from these solutions, we also obtain a broad class of punctures for multiple M5-branes probing general ADE singularities. The essential idea in our approach is to recast the structure of punctures in terms of a dynamical system with position $x(i)$ and momentum $p(i)$

in which evolution in time corresponds to moving from one node of an affine A-type quiver to its neighbor. Classification of regular punctures (namely simple poles) thus reduces to determining which initial conditions produce periodic orbits of this dynamical system. Higher-order poles for punctures follow recursively from the lower-order pole solutions. We have shown that for periodic orbits, the momenta always take values in the rational numbers and furthermore satisfy the condition $p(i) = a(i)/b$ with $a(i), b$ relatively prime integers and b not divisible by 4. Moreover, the resulting dynamical system exhibits a remarkable sensitivity to initial conditions. In the remainder of this section, we discuss some future avenues for investigation.

One direction which would clearly be interesting to understand better would be the structure of regular punctures for a single M5-brane probing a D- or E-type singularity, and in particular the associated dynamical system. At least for D-type theories, there is a similar notion of "long time evolution." From this perspective, the fact that the E-type theories have a small number of nodes suggests that it should be possible to fully classify this case.

From a conceptual point of view, it is quite tempting to interpret the time evolution of our dynamical system directly in the geometry of the target space. Indeed, we can identify the Taub-NUT circle of the resolution of $\mathbb{C}^2/\mathbb{Z}_k$ with this time coordinate. Along these lines, we have also seen that at least for sufficiently long orbits (namely for appropriate choices of the initial conditions), the analytic behavior of the dynamical system greatly simplifies. Geometrically, this appears to correspond to a limit where the orbifold $\mathbb{C}^2/\mathbb{Z}_k$ collapses to an $\mathbb{R}^3$. The T-dual description is also illuminating as it takes us to a large number of parallel NS5-branes. It would be interesting to understand the arithmetic properties of the dynamical system from this perspective.

In the large N limit of many M5-branes, these probe theories have holographic duals of the form $AdS_7 \times S^4/\Gamma$ (see, e.g., [16,17,22]), and compactification on a Riemann surface with punctures has been studied in part in [50,59,60]. As we have already remarked, we can take our dynamical system and embed it into higher-rank theories. It would be very interesting to understand the holographic description of this dynamical system.

Finally, we have seen that the structure of the punctures depends in a very sensitive way on the initial momentum $p(1)$ of the dynamical system. Indeed, the sort of branching behavior exhibited in Fig. 5 is reminiscent of the ultrametric trees which appear in some measures of complexity for spin glasses, and certain enumeration problems connected with string vacua (see, e.g., [61]). Here, we have found a very concrete and well-controlled example of this phenomenon in compactifications of 6D SCFTs. The surprising complexity thus obtained would be exciting to further quantify.

Acknowledgements We thank F. Apruzzi, J. Marincel, N. Miller and T. Rudelius for helpful discussions. JJH thanks the 2017 Summer Workshop at the Simons Center for Geometry and Physics as well as the Aspen Center for Physics Winter Conference in 2017 on Superconformal Field Theories in $d \geq 4$, NSF Grant PHY-1066293, for hospitality during part of this work. The work of FH and JJH is supported by NSF CAREER Grant PHY-1756996. The work of FH is also supported by NSF Grant PHY-1620311.

A Periodic orbit proofs

With notation as in Sect. 3.4, in this Appendix we establish that for an eternal puncture with initial momentum $p(1) = a/b$ with a, b coprime, when $b \neq 0 \bmod 4$, we always obtain a periodic orbit.

We first establish some important properties of the leading-order contribution to the dynamical system, as given in Eq. 3.56.

Lemma 1 *Let $p = a/b$ where $a > 0$ and $b > 0$ are coprime. If $b \bmod 4 \neq 0$, there exists a periodic orbit for the leading contribution $\Delta_{\mathrm{L}}^{(m)}$ which is independent of the initial value $\Delta_{\mathrm{L}}^{(1)}$. The number of extrema in this orbit is given by*

$$k' = \begin{cases} b & b \text{ is even} \\ 2b & b \text{ is odd} \end{cases} \tag{A.1}$$

for which we have

$$\Delta_{\mathrm{L}}^{(m+k')} = \Delta_{\mathrm{L}}^{(m)}. \tag{A.2}$$

Proof of Lemma 1 In order to proof this lemma, we have to show that

$$2k'p + \sum_{l=0}^{k'-1} (-1)^l \,\mathrm{Ceil}(\Delta_{\mathrm{L}}^{(m)} + 2lp) = 0 \tag{A.3}$$

holds under the assumptions stated in the lemma. If this is the case, (A.2) follows directly from (3.56). Most of the terms in the sum cancel due to the alternating sign. If we only keep the non-vanishing contributions, the equation we have to check can be rewritten as

$$2k'p + \sum_{l=0}^{k'-1} (-1)^l \,\mathrm{Ceil}(\Delta_{\mathrm{L}}^{(m)} + 2lp) = \sum_{l=0}^{2k'p-1} \mathrm{sgn}_-\,(2p - (l \bmod 4p)) = 0 \tag{A.4}$$

with

$$\mathrm{sgn}_-(x) = \begin{cases} 1 & x > 0 \\ -1 & x \leq 0. \end{cases} \tag{A.5}$$

The argument of the sgn_- function has the point symmetry

$$2p - ((l_* + l) \bmod 4p) = -2p + ((l_* - l) \bmod 4p) \quad \forall\, l \in \mathbb{N},\ 0 < l < 2k'p - l_* \tag{A.6}$$

around the point

$$l_* = \begin{cases} a & \text{for } b \bmod 2 = 0 \\ 2a & \text{for } b \bmod 2 \neq 0. \end{cases} \tag{A.7}$$

Hence, there are even more terms in the sum (A.4) which cancel, too. Finally, one is left with

$$\sum_{l=0}^{2k'p-1} \mathrm{sgn}_-\,(2p-(l \bmod 4p)) = \sum_{l\in\{0,\,l_*\}} \mathrm{sgn}_-\,(2p-(l \bmod 4p)) = \mathrm{sgn}_-(2p)-\mathrm{sgn}_-(0) = 1-1 = 0. \tag{A.8}$$

Lemma 2 *Let $p = a/b$ where $a > 0$ and $b > 0$ are coprime. If $b \bmod 4 = 0$, $\Delta_{\mathrm{L}}^{(m)}$ is shifted by 1 after $b/2$ time steps*

$$\Delta_{\mathrm{L}}^{(m+b/2)} = \Delta_{\mathrm{L}}^{(m)} + 1. \tag{A.9}$$

Proof of Lemma 2 The proof for this lemma requires only a very slight modification of the previous proof. Instead of (A.3), we now want to show that

$$bp + \sum_{l=0}^{b/2-1} (-1)^l\,\mathrm{Ceil}(\Delta_{\mathrm{L}}^{(m)} + 2lp) = 1 \tag{A.10}$$

holds. Again, we rewrite this sum as

$$bp + \sum_{l=0}^{b/2-1} (-1)^l\,\mathrm{Ceil}(\Delta_{\mathrm{L}}^{(m)} + 2lp) = \sum_{l=0}^{bp-1} \mathrm{sgn}_-\,(2p-(l \bmod 4p)) = 1 \tag{A.11}$$

and take advantage of the point symmetry of the argument of the sgn_ function. Now, $l_* = a/2$ and therewith not an integer. Thus, instead of two contributions to the same which cancel each other, we find

$$bp + \sum_{l=0}^{b/2-1} (-1)^l\,\mathrm{Ceil}(\Delta_{\mathrm{L}}^{(m)} + 2lp) = \mathrm{sgn}_-(2p) = 1. \tag{A.12}$$

Now consider a periodic orbit $\{\Delta_{\mathrm{L}}^{(1)}, \ldots, \Delta_{\mathrm{L}}^{(k')}\}$ which arises from Lemma 1 and take instead of $\Delta_{\mathrm{L}}^{(1)}$, $\Delta_{\mathrm{L}}^{(2)}$ as the initial condition. In this case, we obtain another periodic orbit $\{\Delta_{\mathrm{L}}^{(2)}, \ldots, \Delta_{\mathrm{L}}^{(k')}, \Delta_{\mathrm{L}}^{(1)}\}$. The only difference between the two of them is that all elements are shifted to the right by one position. Periodic orbits which arise from such shifts are members of the same equivalence class. All their relevant properties do not change within the class. Hence, it is sufficient to study only one representative of each equivalence class.

Lemma 3 *A unique representative of each equivalence class for periodic orbits $\Delta_{\mathrm{L}}^{(m)}$ which arise from Lemma 1 is given by the initial conditions*

$$0 < |\Delta_{\mathrm{L}}^{(1)}| < \frac{1}{k'} \tag{A.13}$$

for $p = a/b$, $a > 0$ and $b > 0$. For all other remaining $\Delta_{\mathrm{L}}^{(m)}$ in this orbit, we instead have:

$$\left| \left(\Delta_{\mathrm{L}}^{(m)} + \frac{1}{2} \right) \mathit{mod}\, 1 - \frac{1}{2} \right| > \frac{1}{k'} \quad \forall\, m \in \{2, \ldots, k'/2, k'/2+2, \ldots, k'\} \tag{A.14}$$

and

$$\left| \left(\Delta_{\mathrm{L}}^{(k'/2+1)} + \frac{1}{2} \right) \mathit{mod}\, 1 - \frac{1}{2} \right| < \frac{1}{k'}. \tag{A.15}$$

Proof of Lemma 3 First, we prove that from the representatives (A.13) all other orbits of the same equivalence class can be obtained by shifting the time evolution. More specifically, we shift by n steps to the left

$$\Delta_{\mathrm{L}}^{\prime(m)} = \Delta_{\mathrm{L}}^{(m+2n)} - 2\,\mathrm{Floor}\left(\frac{\Delta_{\mathrm{L}}^{(1+2n)} + 1}{2} \right) \tag{A.16}$$

and perform an additional integer shift to keep $\Delta^{\prime(1)}$ in the fixed interval $(-1, 1)$. According to (3.54), this interval covers all possible initial conditions. A shift by an integer leaves the iteration (3.53) for the leading contributions $\Delta_{\mathrm{L}}^{(m)}$ invariant and therefore does not change the equivalence class of the orbit. After this transformation, we obtain

$$\Delta_{\mathrm{L}}^{\prime(1)} = (\Delta_{\mathrm{L}}^{(1)} + 2np + 1) \bmod 2 - 1. \tag{A.17}$$

as new initial condition. Sweeping n from 1 to k', we find that all initial conditions fill the lattice

$$\Delta_{\mathrm{L}}^{\prime(1)} \in \left\{ -1 + 1/k' + \Delta_{\mathrm{L}}^{(1)},\ -1/2 + 3/k' + \Delta_{\mathrm{L}}^{(1)}, \ldots, 1 - 1/k' + \Delta_{\mathrm{L}}^{(1)} \right\}. \tag{A.18}$$

Varying also $\Delta_{\mathrm{L}}^{(1)}$ in the bounds given by (A.13), we eventually see that

$$\forall\, \Delta_{\mathrm{L}}^{\prime(1)} \in (-1, 1) \quad \exists\, n \in \{1, \ldots, k'\} \text{ and } \Delta_{\mathrm{L}}^{(1)} \in \left(-\frac{1}{k'}, \frac{1}{k'} \right) \text{ s.t. (A.17) holds.} \tag{A.19}$$

This proves the first part of the lemma.

In order to prove the second part, we first note that

$$\left(\Delta_{\mathrm{L}}^{(m)} + \frac{1}{2} \right) \bmod 1 = \left(\Delta_{\mathrm{L}}^{(1)} + 2(m-1)p + \frac{1}{2} \right) \bmod 1 \quad \forall\, m \in \mathbb{Z}, \tag{A.20}$$

which follows from (3.53) after stripping off all integer contributions. Because

$$k'p \in \mathbb{N}, \tag{A.21}$$

we immediately find that

$$\left(\Delta_{\mathrm{L}}^{(m+k'/2)}+\frac{1}{2}\right) \bmod 1=\left(\Delta_{\mathrm{L}}^{(m)}+\frac{1}{2}\right) \bmod 1 \tag{A.22}$$

holds. Under the assumption (A.13), this relation directly implies (A.15). More generally,

$$\left(\Delta_{\mathrm{L}}^{(1)}+2(m-1)p+\frac{1}{2}\right) \bmod 1-\frac{1}{2} \in \Lambda_{k'}(\Delta_{\mathrm{L}}^{(1)}) \tag{A.23}$$

only takes values on the lattice

$$\Lambda_{k'}(\Delta)=\{-1/2+1/k'+\Delta,\ -1/2+3/k'+\Delta, \ldots, 1/2-1/k'+\Delta\}, \tag{A.24}$$

with $|\Delta| < 1/k'$. This lattice has exactly $k'/2$ elements, and for $m \in \{1, \ldots, k'/2\}$, every one occurs exactly one times. There is only one element in this lattice whose absolute value is small that $1/k'$. This element is Δ. It arises for $m = 0$ from (A.23). All other elements have an absolute value which is larger that $1/k'$. This proves (A.14) for $m \in \{2, \ldots, k'/2\}$. The remaining conditions follow immediately from (A.22). □

We call this canonical representative an aligned periodic orbit:

Definition 1 A periodic orbit ($p = a/b$, a, b coprime and $b \bmod 4 \neq 0$) with

$$0 < |\Delta_{\mathrm{L}}^{(1)}| < \frac{1}{k'} \tag{A.25}$$

is called aligned.

A direct consequence of Lemma 3 is that every orbit can be aligned by a suitable shift.

Lemma 4 *Let $\Delta_{\mathrm{L}}^{(m)}$ capture a periodic orbit which arises from Lemma 1. All $\Delta_{\mathrm{L}}^{(m)}$ are bounded by*

$$|\Delta_{\mathrm{L}}^{(m)}| < k'p+2 = \begin{cases} a+1 & \text{for } b \text{ even} \\ 2a+1 & \text{for } b \text{ odd.} \end{cases} \tag{A.26}$$

Proof of Lemma 4 First, we deduce for (3.53) that

$$|\Delta^{(m+1)}| < |\Delta^{(m)}| + 1 \tag{A.27}$$

holds. In order to prove the lemma, we now show that

$$|\Delta^{(1+2n)}| < k'p+1 \quad \forall n \in \mathbb{Z}. \tag{A.28}$$

As in the proofs of the Lemmas 1 and 2, we write the expression for $\Delta_{\mathrm{L}}^{(1+2n)}$ in (3.56) as

$$\Delta_{\mathrm{L}}^{(1+2n)} = (\Delta_{\mathrm{L}}^{(1)}+4np) \bmod 1 + \sum_{l=0}^{\mathrm{Floor}(4np)-1} \mathrm{sgn}_{-}\,(2p-(l \bmod 4p)). \tag{A.29}$$

For $n = k'/2$, the sum on the right-hand side vanishes according to Lemma 1. Moreover, the sgn_ function can only take values of 1 or -1. Hence, the sum is bounded by

$$\left| \sum_{l=0}^{\text{Floor}(4np)-1} \text{sgn\_}\,(2p - (l \bmod 4p)) \right| < k'p \quad \forall n \in \mathbb{Z}. \tag{A.30}$$

Taking into account the first part of (A.29) too, we see that (A.28) holds. This completes the proof. □

Let us now start to analyze the effect of the corrections $\delta^{(m)}$ in (3.51) for the case where the leading contributions $\Delta_{\text{L}}^{(m)}$ describe an aligned, periodic orbit defined in definition 1. In this discussion, the functions $\delta_1(\Delta, y)$, $\delta_2(\Delta, y)$ and $\tilde{\delta}_2(\Delta, y)$, which we defined in (3.45), (3.47) and (3.50), play an important role. Under the assumption that Δ is bound by

$$|\Delta| < \Delta_{\text{B}}, \tag{A.31}$$

we can bound them from above by

$$|\delta_1(\Delta, y)| < \frac{(2\Delta_{\text{B}} + 2)^2}{2(l-1)}, \quad |\delta_2(\Delta, y)| < \frac{(2\Delta_{\text{B}} + 2)^2}{2(l-1)}$$
$$\text{and} \quad |\tilde{\delta}_2(\Delta, y)| < \frac{(2\Delta_{\text{B}} + 2)^2}{2(l-1)}. \tag{A.32}$$

We want to guarantee that the subleading part $|\delta^{(m)}|$ is small and does not change the qualitative behavior of the time evolution. If this is the case, the time evolution is governed by the leading contributions $\Delta_{\text{L}}^{(m)}$ for which we already proved an analytic expression in (3.56). More specifically, $|\delta^{(m)}|$ has to be smaller than a certain boundary $\delta_{\text{B}} < 1$, at least for the first $k'/2$ steps. Thus, we require

$$|\delta^{(m)}| < \delta_{\text{B}} \quad \text{and} \quad |\Delta^{(m)}| < \Delta_{\text{B}} \quad \forall m \in \{1, \ldots, k'/2 + 1\} \tag{A.33}$$

and fix δ_{B} such that

$$\text{Ceil}(\Delta_{\text{L}}^{(m)}) = \text{Ceil}\big(\Delta^{(m)} + \delta_1(\Delta^{(m)}, y^{(m)})\big) \quad \forall m \in \{1, \ldots, k'/2\} \tag{A.34}$$

is not violated. If it would be violated, then $|\delta^{(m)}|$ would be immediately bigger than one and our analysis would break down. For $m = 1$, we have

$$\text{Ceil}(\Delta_{\text{L}}^{(1)}) = \text{Ceil}\big(\Delta_{\text{L}}^{(1)} - \delta_1(\Delta^{(1)}, y^{(1)}) + \delta_1(\Delta^{(1)}, y^{(1)})\big) = \text{Ceil}(\Delta_{\text{L}}^{(1)}) \tag{A.35}$$

automatically. For $m = 2$, we obtain the constraint

$$\text{Ceil}(\Delta_{\text{L}}^{(2)}) = \text{Ceil}\big(\Delta_{\text{L}}^{(2)} + \delta^{(2)} + \delta_1(\Delta^{(2)}, y^{(2)})\big) = \text{Ceil}(\Delta_{\text{L}}^{(2)}), \tag{A.36}$$

where

$$|\delta^{(2)}| \leq |\delta^{(1)} + \delta_2(\Delta^{(1)}, y^{(1)})| < 2\frac{(2\Delta_B + 2)^2}{2(l-1)} \tag{A.37}$$

after taking into account the bounds (A.32). This constraint only holds, if we restrict the domain of allowed values for $\Delta_L^{(2)}$ to

$$\left|\left(\Delta_L^{(2)} + \frac{1}{2}\right) \bmod 1 - \frac{1}{2}\right| \geq 3\frac{(2\Delta_B + 2)^2}{2(l-1)}. \tag{A.38}$$

Repeating this reasoning step for step, we eventually find

$$\bigwedge_{m=2}^{k'/2} \left|\left(\Delta_L^{(m)} + \frac{1}{2}\right) \bmod 1 - \frac{1}{2}\right| \geq (m+1)\frac{(2\Delta_B + 2)^2}{2(l-1)}, \tag{A.39}$$

which implies

$$|\delta^{(k'/2+1)}| < k'\frac{(\Delta_B + 1)^2}{l-1} = \delta_B. \tag{A.40}$$

For the following discussion, it is sufficient to use the weaker, but simpler version

$$\left|\left(\Delta_L^{(m)} + \frac{1}{2}\right) \bmod 1 - \frac{1}{2}\right| \geq (k'+2)\frac{(\Delta_B + 1)^2}{l-1} = \delta_B \quad \forall m \in \{2, \ldots, k'/2\}. \tag{A.41}$$

If it holds, the subleading part $\delta^{(m)}$ is given by

$$\delta^{(m)} = \delta^{(1)} + \sum_{n=1}^{m-1} \delta_2\big(\Delta_L^{(n)}, y^{(n)}\big) \quad \text{for} \quad \forall m \in \{2, \ldots, k'/2+1\}. \tag{A.42}$$

Taking into account Lemma 3, we know that:

$$\left|\left(\Delta_L^{(m)} - \frac{1}{2}\right) \bmod 1 + \frac{1}{2}\right| > \frac{1}{k'}. \tag{A.43}$$

On the other hand, the constraint (A.41) also tells us that:

$$\delta_B \leq \left|\left(\Delta_L^{(m)} - \frac{1}{2}\right) \bmod 1 + \frac{1}{2}\right|. \tag{A.44}$$

Scanning over the admissible values of δ_B, we see that the largest δ_B which will satisfy line A.43 satisfies the inequality:

$$\delta_B \leq \frac{1}{k'}. \tag{A.45}$$

If we furthermore combine Lemma 4 with $|\delta^{(m)}| < \delta_B < 1$ for $m \in \{1, \ldots, k'/2\}$, we see that there are two additional inequalities we can write:

$$|\Delta^{(m)}| < \Delta_B \tag{A.46}$$

$$|\Delta^{(m)}| \leq |\Delta_{\mathrm{L}}^{(m)}| + |\delta^{(m)}| < k'p + 3 \quad \forall\, m \in \{2, \ldots, k'/2\} \tag{A.47}$$

hold. Again, we seek out the largest value of Δ_B compatible with these two conditions. This is fixed by taking:

$$\Delta_{\mathrm{B}} = k'p + 3. \tag{A.48}$$

Hence, we can express both boundaries δ_{B} and Δ_{B} in (A.33) in terms of k' and p.

So far we just discussed the subleading part $\delta^{(m)}$ for the first half of the periodic orbit. To go beyond $\Delta^{(k'/2+1)}$ is more involved, because according to Lemma 3

$$\left| \left(\Delta_{\mathrm{L}}^{(k'/2+1)} + \frac{1}{2} \right) \bmod 1 - \frac{1}{2} \right| < \frac{1}{k'} \tag{A.49}$$

holds and enables us to apply the bounds discussed above. There are now two ways one could go. First one could improve the analysis of the contributions from $\delta_1(\Delta, y)$ and $\delta_2(\Delta, y)$. We only used very crude bounds. They worked well for the analysis of the first $k'/2$ corrections $\delta^{(m)}$ but are insufficient as soon as one want to go beyond the special point $k'/2+1$. Alternatively, we can avoid this point completely by approaching the second part of the orbit with the inverse iteration prescription (3.49). In analogy with (A.33), one now requires

$$|\delta^{(m)}| < \delta_B \quad \text{and} \quad |\Delta^{(m)}| < \Delta_B \quad \forall\, m \in \{-k'/2 + 1, \ldots, 0\}. \tag{A.50}$$

As before, we again require

$$\mathrm{Ceil}(\Delta_{\mathrm{L}}^{(m)}) = \mathrm{Ceil}\big(\Delta^{(m)} + \delta_1(\Delta^{(m)}, y^{(m)})\big) \quad \forall\, m \in \{-k'/2 + 1, \ldots, 0\} \tag{A.51}$$

in order to keep $\delta^{(m)}$ smaller than one. Following the same reasoning as above, we find that this constraint is fulfilled when:

$$\delta_{\mathrm{B}} = (k' + 2)\frac{(\Delta_{\mathrm{B}} + 1)^2}{l - 1} \leq \frac{1}{k'} \tag{A.52}$$

with the Δ_{B} in (A.48). Alternatively, we can also state this inequation for l, resulting in

$$1 + k'(k' + 2)(k'p + 4)^2 \leq l. \tag{A.53}$$

If it is satisfied, the corrections for the second part of the orbits are given by

$$\delta^{(m)} = \delta^{(1)} + \sum_{n=m+1}^{1} \tilde{\delta}_2\big(\Delta_{\mathrm{L}}^{(n)}, y^{(n)}\big) \quad \text{for} \quad \forall\, m \in \{-k'/2 + 1, \ldots, 0\}. \tag{A.54}$$

We call the corresponding periodic orbits dominant orbits.

Definition 2 Orbits with $p = a/b$ where a, b are coprime and $b \bmod 4 \neq 0$ are called dominant if they fulfill

$$l \geq 9 + 2k'p + k'(k'+2)(k'p+4)^2 = \begin{cases} 9 + 2a + b(b+2)(a+4)^2 & \text{for } b \text{ even} \\ 9 + 4a + 4b(b+1)(2a+4)^2 & \text{for } b \text{ odd.} \end{cases} \tag{A.55}$$

Note that this definition also takes orbits into account which are not aligned. To this end, we require that not only $l^{(1)} = l$ satisfies the bound (A.53) but all $l^{(m)}$. For dominant orbits, we can now establish

Lemma 5 *For dominant orbits, the subleading part is given by*

$$\delta^{(m)} = \delta^{(1)} + \sum_{n=1}^{m-1} \delta_2\big(\Delta_{\mathrm{L}}^{(n)}, y^{(n)}\big) \quad \textit{for} \quad \forall\, m \in \{2, \ldots, k'/2+1\} \tag{A.56}$$

and

$$\delta^{(m)} = \delta^{(1)} + \sum_{n=m+1}^{1} \tilde{\delta}_2\big(\Delta_{\mathrm{L}}^{(n)}, y^{(n)}\big) \quad \textit{for} \quad \forall\, m \in \{-k'/2+1, \ldots, 0\}. \tag{A.57}$$

After all this preparation, we can finally state the important theorems for dominant periodic orbits.

Theorem 1 *Dominant orbits are periodic and contain k' (given by (A.1)) extrema.*

Proof In order to prove that we indeed have a periodic orbit, we have to show that

$$\Delta^{(-k'/2+1)} = \Delta^{(k'/2+1)} \tag{A.58}$$

holds. This relation is equivalent to

$$\Delta_{\mathrm{L}}^{(-k'/2+1)} + \delta^{(-k'/2+1)} = \Delta_{\mathrm{L}}^{(k'/2+1)} + \delta^{(k'/2+1)}. \tag{A.59}$$

For Lemma 1, we know that $\Delta_{\mathrm{L}}^{(-k'/2+1)} = \Delta_{\mathrm{L}}^{(k'/2+1)}$ holds. Therefore, we only have to show $\delta^{(-k'/2+1)} = \delta^{(k'/2+1)}$ which is equivalent to

$$\sum_{n=-k'/2+2}^{1} \tilde{\delta}_2(\Delta_{\mathrm{L}}^{(n)}, y^{(n)}) = \sum_{n=1}^{k'/2} \delta_2(\Delta_{\mathrm{L}}^{(n)}, y^{(n)}). \tag{A.60}$$

First, we note that Lemma 1 implies

$$\sum_{n=-k'/2+2}^{1} \tilde{\delta}_2(\Delta_{\mathrm{L}}^{(n)}, y^{(n)}) = \sum_{n=k'/2+2}^{k'+1} \tilde{\delta}_2(\Delta_{\mathrm{L}}^{(n)}, y^{(n)}) \tag{A.61}$$

and furthermore

$$\tilde{\delta}_2(\Delta_{\mathrm{L}}^{(n)}, y^{(n)}) = -\delta_2(\Delta_{\mathrm{L}}^{(n-1)}, y^{(n-1)}) \tag{A.62}$$

follows form the definitions (3.47), (3.50) and the iteration prescription (3.53) for the leading contribution. Therefore (A.60) is equivalent to

$$\begin{aligned} 0 &= \sum_{n=1}^{k'} \delta_2(\Delta_{\mathrm{L}}^{(n)}, y^{(n)}) \\ &= \frac{2}{l-1} \sum_{n=0}^{k'/2-1} \left[3\mathrm{Ceil}(\Delta_{\mathrm{L}}^{(2n+1)}) - \mathrm{Ceil}(\Delta_{\mathrm{L}}^{(2n+1)} + 2p) - 1\right] \\ &\quad \times \left[2p + \mathrm{Ceil}(\Delta_{\mathrm{L}}^{(2n+1)}) - \mathrm{Ceil}(\Delta_{\mathrm{L}}^{(2n+1)} + 2p)\right]. \end{aligned} \tag{A.63}$$

After introducing

$$s^{(n)} = \mathrm{Ceil}(\Delta_{\mathrm{L}}^{(1)} + 4pn) - \mathrm{Ceil}(\Delta_{\mathrm{L}}^{(1)} + 4pn + 2p), \tag{A.64}$$

this equation is equivalent to

$$0 = \sum_{n=0}^{k'/2-1} 2\mathrm{Ceil}(\Delta_{\mathrm{L}}^{(2n+1)})(2p + s^{(n)}) + \sum_{n=0}^{k'/2-1} (2p + s^{(n)})(s^{(n)} - 1). \tag{A.65}$$

Writing (3.56) as

$$\Delta_{\mathrm{L}}^{(1+2n)} = \Delta_{\mathrm{L}}^{(1)} + 2\sum_{l=0}^{n-1} s^{(l)}, \tag{A.66}$$

Lemma 1 implies

$$\sum_{l=0}^{k'/2+1} s^{(l)} = -k'p. \tag{A.67}$$

Moreover, we take into account that $(s^{(l)})^2 = -s^{(l)}$. Thus, (A.60) is equivalent to

$$\begin{aligned} \sum_{n=0}^{k'/2-1} \mathrm{Ceil}(\Delta_{\mathrm{L}}^{(2n+1)})(2p + s^{(n)}) &= \sum_{n=0}^{k'/2-1} \left(\mathrm{Ceil}(\Delta_{\mathrm{L}}^{(1)} + 4pn) + 2\sum_{l}^{n-1} s^{(l)}\right)\left(2p + s^{(n)}\right) \\ &= \frac{k'p}{2}(2p-1). \end{aligned} \tag{A.68}$$

All what remains is to calculate the four remaining sums on the right-hand side in the first line. Let us start with

$$2p\sum_{n=0}^{k'/2-1}\mathrm{Ceil}(\Delta_{\mathrm{L}}^{(1)}+4pn)=\frac{k'p}{2}(2k'p+1)-2k'p^2+p\,\mathrm{sgn}\,\Delta_{\mathrm{L}}^{(1)}\quad\text{for}\quad 0<|\Delta_{\mathrm{L}}^{(1)}|<\frac{1}{k'}. \tag{A.69}$$

In order to better understand this result, assume for a moment that $\Delta_{\mathrm{L}}^{(1)}=0$. Now

$$\mathrm{Ceil}(4np)+\mathrm{Ceil}\left(4(k'/2-n)p\right)=2k'p+1 \tag{A.70}$$

holds. We find this contribution exactly $k'/4-1/2$ times in the sum in (A.69). If $|\Delta_{\mathrm{L}}^{(1)}|<1/k'$ instead of being zero, it only affects the summand for $n=0$ and therefore gives rise to the sgn function in (A.69). Second, we evaluate the sum

$$2\sum_{n=0}^{k'/2-1}\sum_{l=0}^{n-1}s^{(n)}s^{(l)}=2\sum_{n=1}^{k'p}(n-1)=k'p(k'p-1). \tag{A.71}$$

Thus, we finally need to show that

$$\sum_{n=0}^{k'/2-1}\left(\mathrm{Ceil}(\Delta_{\mathrm{L}}^{(1)}+4pn)s^{(n)}+4p\sum_{l=0}^{n-1}s^{(l)}\right)=-k'p(2k'p-3p)-p\mathrm{sgn}\,(\Delta_{\mathrm{L}}^{(1)}) \tag{A.72}$$

holds. To do, let us consider the following problem: Choose $i=1,\ldots,k'p$ integers $0\le m_i\le 2k'p$ such that they fulfill

$$\exists\, n_i\in\mathbb{N}\ \text{s.t.}\ \Delta_{\mathrm{L}}^{(1)}+4pn_i<m_i<\Delta_{\mathrm{L}}^{(1)}+4pn_i+2p. \tag{A.73}$$

In terms of these integers, we can write (A.72) as

$$\sum_{i=1}^{k'p}\left(4p\,\mathrm{Ceil}\left(\frac{m_i-\Delta_{\mathrm{L}}^{(1)}}{4p}\right)-m_i-2k'p\right)=-k'p(2k'p-3p)-p\,\mathrm{sgn}\,(\Delta_{\mathrm{L}}^{(1)}) \tag{A.74}$$

which simplifies to

$$4\sum_{i=1}^{k'p}\left(\frac{m_i-\Delta_{\mathrm{L}}^{(1)}}{4p}\bmod 1\right)=k'p+\mathrm{sgn}\,\Delta_{\mathrm{L}}^{(1)}-\Delta_{\mathrm{L}}^{(1)}k'. \tag{A.75}$$

To see that this relations is indeed fulfilled, we again check first the case for $\Delta_{\mathrm{L}}^{(1)}=0$. In this case, it is easy to check that if an integer m satisfies (A.73), there is another integer

$$m'=(k'p-m)\bmod 2k'p \tag{A.76}$$

which does so, too. Let us add up this two contributions to the sum on the left-hand side of (A.75):

$$\frac{m}{4p} \bmod 1 + \left(\frac{k'}{4} - \frac{m}{4p}\right) \bmod 1 = \frac{1}{2}. \tag{A.77}$$

Here, we have used that

$$\frac{k'}{4} \bmod 1 = \frac{1}{2} \quad \text{and} \quad 0 \leq \frac{m}{4p} \bmod < \frac{1}{2}, \tag{A.78}$$

which follows directly from (A.73). This situation occurs $k'p/2$ times, and we reproduces (A.75) for $\Delta_{\mathrm{L}}^{(1)} = 0$. For $|\Delta_{\mathrm{L}}^{(1)}| < \frac{1}{k'}$, the deviations from this argumentation are minor. It is straightforward to check that they reproduce exactly the remaining terms on the right-hand side of (A.75). □

Corollary 1 *All orbits with $p = a/b$ with a, b coprime and $b \bmod 4 \neq 0$ are periodic.*

Proof We prove this statement by contradiction. Assume we start from a $y^{(1)}$ which does not give rise to a periodic orbit. Of course this $y^{(1)}$ cannot be the initial condition of a dominant orbit because these are periodic. Thus,

$$|y^{(1)}| < y_{\max} \tag{A.79}$$

is bounded from above (with increasing $|y^{(1)}|$ also l increases gradually and at some point would fulfill the requirement in definition 2 for a dominant orbit). Moreover, we note that $y^{(m)}$ can only change in multiples of $1/b$ according to (3.35). As the sequence $y^{(m)}$ does not describes a periodic orbit, all $y^{(m)}$ are unique and cannot repeat. These two observations give rise to

$$\exists\, y \in \{y^{(2)}, \ldots, y^{(N)}\} \quad \text{with} \quad |y - y^{(1)}| \geq \frac{N}{2b}, \tag{A.80}$$

which implies

$$|y| \geq \frac{N}{2b} - y_{\max}. \tag{A.81}$$

For $N = \mathrm{Ceil}(4by_{\max})$, there exists an y in the first N elements of the time evolution which is bigger than $y_{\max}$. This is a contradiction. Such a y implies a periodic, dominant orbit, but we started with the assumption that the orbit is not periodic. □

Theorem 2 *Let $x^{(i)}$ describe a dominant, aligned, periodic orbit. Its length, which is defined as*

$$x(i) = x(i + k), \tag{A.82}$$

is

$$k = k'(l + 2p) = \begin{cases} lb + 2a & \text{for } b \text{ even} \\ 2lb + 4a & \text{for } b \text{ odd}. \end{cases} \tag{A.83}$$

Proof The length of the orbit is given by

$$k = \sum_{l=1}^{k'} l^{(m)} = \sum_{l=0}^{k'/2-1} \left[l^{(1+2l)} + l^{(2+2l)} \right]. \tag{A.84}$$

It is straightforward to check that

$$l^{(m)} + l^{(m+1)} = 2l - 2\mathrm{Ceil}(\Delta_{\mathrm{L}}^{(m)}) + 2\mathrm{Ceil}(\Delta_{\mathrm{L}}^{(m)} + 2p) \tag{A.85}$$

follows from (3.44). It allows us to write

$$k = lk' - \sum_{l=0}^{k'-1} (-1)^l \,\mathrm{Ceil}(\Delta_{\mathrm{L}}^{(1)} + 2lp) = lk' + \Delta_{\mathrm{L}}^{(1)} - \Delta_{\mathrm{L}}^{(1+k')} + 2k'p \tag{A.86}$$

after taking into account (3.56). According to Lemma 1, the part $\Delta_{\mathrm{L}}^{(1)} - \Delta_{\mathrm{L}}^{(1+k')}$ vanishes. □

References

1. Witten, E.: String theory dynamics in various dimensions. Nucl. Phys. B **443**, 85–126 (1995). arXiv:hep-th/9503124
2. Witten, E.: Some comments on string dynamics. In: Future Perspectives in String Theory. Proceedings, Conference, Strings'95, Los Angeles, USA, March 13–18, 1995 (1995). arXiv:hep-th/9507121
3. Strominger, A.: Open p-branes. Phys. Lett. B **383**, 44–47 (1996). arXiv:hep-th/9512059
4. Seiberg, N.: Nontrivial fixed points of the renormalization group in six-dimensions. Phys. Lett. B **390**, 169–171 (1997). arXiv:hep-th/9609161
5. Witten, E.: Small instantons in string theory. Nucl. Phys. B **460**, 541–559 (1996). arXiv:hep-th/9511030
6. Ganor, O.J., Hanany, A.: Small E_8 instantons and tensionless noncritical strings. Nucl. Phys. B **474**, 122–140 (1996). arXiv:hep-th/9602120
7. Morrison, D.R., Vafa, C.: Compactifications of F-theory on Calabi–Yau threefolds—II. Nucl. Phys. B **476**, 437–469 (1996). arXiv:hep-th/9603161
8. Seiberg, N., Witten, E.: Comments on string dynamics in six-dimensions. Nucl. Phys. B **471**, 121–134 (1996). arXiv:hep-th/9603003
9. Bershadsky, M., Johansen, A.: Colliding Singularities in F-theory and Phase Transitions. Nucl. Phys. B **489**, 122–138 (1997). arXiv:hep-th/9610111
10. Brunner, I., Karch, A.: Branes at orbifolds versus Hanany Witten in six-dimensions. JHEP **03**, 003 (1998). arXiv:hep-th/9712143
11. Blum, J.D., Intriligator, K.A.: Consistency conditions for branes at orbifold singularities. Nucl. Phys. B **506**, 223–235 (1997). arXiv:hep-th/9705030
12. Aspinwall, P.S., Morrison, D.R.: Point-like instantons on K3 orbifolds. Nucl. Phys. B **503**, 533–564 (1997). arXiv:hep-th/9705104
13. Intriligator, K.A.: New string theories in six-dimensions via branes at orbifold singularities. Adv. Theor. Math. Phys. **1**, 271–282 (1998). arXiv:hep-th/9708117
14. Hanany, A., Zaffaroni, A.: Branes and six-dimensional supersymmetric theories. Nucl. Phys. B **529**, 180–206 (1998). arXiv:hep-th/9712145
15. Heckman, J.J., Morrison, D.R., Vafa, C.: On the Classification of 6D SCFTs and Generalized ADE Orbifolds. JHEP **05**, 028 (2014). arXiv:1312.5746 [hep-th]. [Erratum: JHEP 06 (2015) 017]
16. Gaiotto, D., Tomasiello, A.: Holography for (1,0) theories in six dimensions. JHEP **12**, 003 (2014). arXiv:1404.0711 [hep-th]

17. Del Zotto, M., Heckman, J.J., Tomasiello, A., Vafa, C.: 6D conformal matter. JHEP **02**, 054 (2015). arXiv:1407.6359 [hep-th]
18. Del Zotto, M., Heckman, J.J., Morrison, D.R., Park, D.S.: 6D SCFTs and gravity. JHEP **06**, 158 (2015). arXiv:1412.6526 [hep-th]
19. Heckman, J.J., Morrison, D.R., Rudelius, T., Vafa, C.: Atomic classification of 6D SCFTs. Fortsch. Phys. **63**, 468–530 (2015). arXiv:1502.05405 [hep-th]
20. Bhardwaj, L.: Classification of 6D $\mathcal{N} = (1, 0)$ Gauge theories. JHEP **11**, 002 (2015). arXiv:1502.06594 [hep-th]
21. Chang, C.-M., Lin, Y.-H.: Carving out the end of the world or (superconformal bootstrap in six dimensions). JHEP **08**, 128 (2017). arXiv:1705.05392 [hep-th]
22. Apruzzi, F., Fazzi, M., Rosa, D., Tomasiello, A.: All AdS_7 solutions of type II supergravity. JHEP **04**, 064 (2014). arXiv:1309.2949 [hep-th]
23. Heckman, J.J.: More on the matter of 6D SCFTs. Phys. Lett. B **747**, 73–75 (2015). arXiv:1408.0006 [hep-th]
24. Del Zotto, M., Heckman, J.J., Park, D.S., Rudelius, T.: On the defect group of a 6D SCFT. Lett. Math. Phys. **106**(6), 765–786 (2016). arXiv:1503.04806 [hep-th]
25. Gaiotto, D., Razamat, S.S.: $\mathcal{N} = 1$ theories of class $\mathcal{S}_k$. JHEP **07**, 073 (2015). arXiv:1503.05159 [hep-th]
26. Ohmori, K., Shimizu, H., Tachikawa, Y., Yonekura, K.: 6d $\mathcal{N} = (1, 0)$ theories on T^2 and class S theories: Part I. JHEP **07**, 014 (2015). arXiv:1503.06217 [hep-th]
27. Franco, S., Hayashi, H., Uranga, A.: Charting class $\mathcal{S}_k$ territory. Phys. Rev. D **92**(4), 045004 (2015). arXiv:1504.05988 [hep-th]
28. Del Zotto, M., Vafa, C., Xie, D.: Geometric engineering, mirror symmetry and $6d_{(1,0)} \to 4d_{(\mathcal{N}=2)}$. JHEP **11**, 123 (2015). arXiv:1504.08348 [hep-th]
29. Heckman, J.J., Morrison, D.R., Rudelius, T., Vafa, C.: Geometry of 6D RG flows. JHEP **09**, 052 (2015). arXiv:1505.00009 [hep-th]
30. Cordova, C., Dumitrescu, T.T., Intriligator, K.: Anomalies, renormalization group flows, and the a-theorem in six-dimensional (1, 0) theories. JHEP **10**, 080 (2016). arXiv:1506.03807 [hep-th]
31. Hanany, A., Maruyoshi, K.: Chiral theories of class $\mathcal{S}$. JHEP **12**, 080 (2015). arXiv:1505.05053 [hep-th]
32. Aganagic, M., Haouzi, N.: ADE little string theory on a Riemann surface (and triality). arXiv:1506.04183 [hep-th]
33. Louis, J., Lüst, S.: Supersymmetric AdS_7 backgrounds in half-maximal supergravity and marginal operators of (1, 0) SCFTs. JHEP **10**, 120 (2015). arXiv:1506.08040 [hep-th]
34. Ohmori, K., Shimizu, H., Tachikawa, Y., Yonekura, K.: 6D $\mathcal{N} = (1, 0)$ theories on S^1/T^2 and class S theories: part II. JHEP **12**, 131 (2015). arXiv:1508.00915 [hep-th]
35. Coman, I., Pomoni, E., Taki, M., Yagi, F.: Spectral curves of $\mathcal{N} = 1$ theories of class $\mathcal{S}_k$. arXiv:1512.06079 [hep-th]
36. Cremonesi, S., Tomasiello, A.: 6D holographic anomaly match as a continuum limit. JHEP **05**, 031 (2016). arXiv:1512.02225 [hep-th]
37. Heckman, J.J., Rudelius, T., Tomasiello, A.: 6D RG flows and nilpotent hierarchies. JHEP **07**, 082 (2016). arXiv:1601.04078 [hep-th]
38. Cordova, C., Dumitrescu, T.T., Intriligator, K.: Deformations of superconformal theories. JHEP **11**, 135 (2016). arXiv:1602.01217 [hep-th]
39. Morrison, D.R., Vafa, C.: F-theory and $\mathcal{N} = 1$ SCFTs in four dimensions. arXiv:1604.03560 [hep-th]
40. Heckman, J.J., Jefferson, P., Rudelius, T., Vafa, C.: Punctures for theories of class $\mathcal{S}_\Gamma$. JHEP **03**, 171 (2017). arXiv:1609.01281 [hep-th]
41. Cordova, C., Dumitrescu, T.T., Intriligator, K.: Multiplets of superconformal symmetry in diverse dimensions. arXiv:1612.00809 [hep-th]
42. Kim, H.-C., Kim, S., Park, J.: 6D strings from new chiral gauge theories. arXiv:1608.03919 [hep-th]
43. Shimizu, H., Tachikawa, Y.: Anomaly of strings of 6D $\mathcal{N} = (1, 0)$ theories. JHEP **11**, 165 (2016). arXiv:1608.05894 [hep-th]
44. Mekareeya, N., Rudelius, T., Tomasiello, A.: T-branes, anomalies and moduli spaces in 6D SCFTs. arXiv:1612.06399 [hep-th]
45. Del Zotto, M., Lockhart, G.: On exceptional instanton strings. JHEP **09**, 081 (2017). arXiv:1609.00310 [hep-th]
46. Apruzzi, F., Hassler, F., Heckman, J.J., Melnikov, I.V.: From 6D SCFTs to dynamic GLSMs. arXiv:1610.00718 [hep-th]

47. Razamat, S.S., Vafa, C., Zafrir, G.: 4D $\mathcal{N} = 1$ from 6D (1, 0). JHEP **04**, 064 (2017). arXiv:1610.09178 [hep-th]
48. Bah, I., Hanany, A., Maruyoshi, K., Razamat, S.S., Tachikawa, Y., Zafrir, G.: 4D $\mathcal{N} = 1$ from 6D $\mathcal{N} = (1, 0)$ on a torus with fluxes. JHEP **06**, 022 (2017). arXiv:1702.04740 [hep-th]
49. Mitev, V., Pomoni, E.: 2D CFT blocks for the 4D class $\mathcal{S}_k$ theories. JHEP **08**, 009 (2017). arXiv:1703.00736 [hep-th]
50. Bah, I., Passias, A., Tomasiello, A.: AdS_5 compactifications with punctures in massive IIA supergravity. arXiv:1704.07389 [hep-th]
51. Del Zotto, M., Heckman, J.J., Morrison, D.R.: 6D SCFTs and phases of 5D theories. arXiv:1703.02981 [hep-th]
52. Apruzzi, F., Heckman, J.J., Rudelius, T.: Green–Schwarz automorphisms and 6D SCFTs. arXiv:1707.06242 [hep-th]
53. Heckman, J.J., Tizzano, L.: 6D fractional quantum hall effect. arXiv:1708.02250 [hep-th]
54. Kim, H.-C., Razamat, S.S., Vafa, C., Zafrir, G.: E-string theory on Riemann surfaces. arXiv:1709.02496 [hep-th]
55. Razamat, S.S., Zafrir, G.: E_8 orbits of IR dualities. arXiv:1709.06106 [hep-th]
56. Gaiotto, D.: $\mathcal{N} = 2$ dualities. JHEP **08**, 034 (2012). arXiv:0904.2715 [hep-th]
57. Douglas, M.R., Moore, G.W.: D-branes, quivers, and ALE instantons. arXiv:hep-th/9603167
58. Xie, D.: M5 brane and four dimensional $\mathcal{N} = 1$ theories I. JHEP **04**, 154 (2014). arXiv:1307.5877 [hep-th]
59. Gaiotto, D., Maldacena, J.: The gravity duals of $N = 2$ superconformal field theories. JHEP **10**, 189 (2012). arXiv:0904.4466 [hep-th]
60. Apruzzi, F., Fazzi, M., Passias, A., Rota, A., Tomasiello, A.: Six-dimensional superconformal theories and their compactifications from type IIA supergravity. Phys. Rev. Lett. **115**(6), 061601 (2015). arXiv:1502.06616 [hep-th]
61. Denef, F.: TASI lectures on complex structures. In: Proceedings, Theoretical Advanced Study Institute in Elementary Particle Physics (TASI 2010). String Theory and Its Applications: From meV to the Planck Scale: Boulder, Colorado, USA, June 1–25, 2010, pp. 407–512 (2011). arXiv:1104.0254 [hep-th]